

Energy transmission pathways of equatorial waves and associated dissipation process in the Maritime Continent

Yusuke Terada¹ and Yukio Masumoto¹

¹University of Tokyo

December 7, 2022

Abstract

Detailed pathway of wave energy exchange between the Pacific and Indian Oceans through the Indonesian archipelago and associated energy dissipation are investigated by using a reduced gravity model with realistic coastline. The wave energy flux analysis that can be applicable for all latitudes in a linear shallow water system is adopted. The energy fluxes diagnosed from the model outputs for the incoming Rossby waves from the Pacific clearly indicate two major energy pathways to the Indian Ocean; one turning southward in the Halmahera Sea and reaches the Indian Ocean via the Banda Sea and the Timor Passage, the other passing through the Makassar and Lombok Straits. The former route, however, is shifted to the western side of the island chain within the Banda Sea due to energy trapping around the island chain. It is also found that strong energy dissipation occurs along the northern coast of New Guinea when the period of the incoming Rossby wave is shorter than 1.5 year. In the case of the Kelvin waves from the Indian Ocean, it is found that the major energy pathway is through the Lombok and Makassar Straits to the Pacific Ocean. However, there appears another pathway along the eastern side of the Sulawesi Island in the Banda Sea to exit through the Molucca Sea only when the wave period is shorter than about one month. This secondary pathway makes it easier for the wave energy from the Indian Ocean to reach the western Pacific Ocean for the short period waves.

1 **Energy transmission pathways of equatorial waves and**
2 **associated dissipation process in the Maritime**
3 **Continent**

4 **Yusuke Terada¹, Yukio Masumoto^{1,2}**

5 ¹Department of Earth and Planetary Science, Graduate School of Science, The University of Tokyo,
6 Tokyo, Japan

7 ²Application Laboratory, Japan Agency for Marine-Earth Science and Technology, Yokohama, Japan

8 **Key Points:**

- 9 • Detailed wave energy pathways within and near the Maritime Continent are iden-
10 tified for the first time with an energy flux analysis
- 11 • The Rossby waves from the Pacific Ocean with sufficiently short period induce strong
12 energy dissipation before entering the Indonesian Seas
- 13 • A northward energy pathway through the eastern side of the Indonesian Seas ap-
14 pears only for short period waves from the Indian Ocean

Corresponding author: Yusuke Terada, terada@eps.s.u-tokyo.ac.jp

Abstract

Detailed pathway of wave energy exchange between the Pacific and Indian Oceans through the Indonesian archipelago and associated energy dissipation are investigated by using a reduced gravity model with realistic coastline. The wave energy flux analysis that can be applicable for all latitudes in a linear shallow water system is adopted. The energy fluxes diagnosed from the model outputs for the incoming Rossby waves from the Pacific clearly indicate two major energy pathways to the Indian Ocean; one turning southward in the Halmahera Sea and reaches the Indian Ocean via the Banda Sea and the Timor Passage, the other passing through the Makassar and Lombok Straits. The former route, however, is shifted to the western side of the island chain within the Banda Sea due to energy trapping around the island chain. It is also found that strong energy dissipation occurs along the northern coast of New Guinea when the period of the incoming Rossby wave is shorter than 1.5 year. In the case of the Kelvin waves from the Indian Ocean, it is found that the major energy pathway is through the Lombok and Makassar Straits to the Pacific Ocean. However, there appears another pathway along the eastern side of the Sulawesi Island in the Banda Sea to exit through the Molucca Sea only when the wave period is shorter than about one month. This secondary pathway makes it easier for the wave energy from the Indian Ocean to reach the western Pacific Ocean for the short period waves.

Plain Language Summary

Indonesian archipelago connects the Pacific and Indian Oceans at low latitude and play a key role in determining regional and global ocean circulations and climate variability by transporting energy and materials. While there are attempts to estimate gross energy transmission of ocean waves through the archipelago from the Pacific to the Indian Ocean and vice versa, detailed pathway of the wave energy within the archipelago and spatial distribution of large energy dissipation associated with the wave propagation have still been veiled. With a new analysis scheme, we identified detailed pathways of wave energy exchange for the first time and their dependencies on the frequency of the incoming wave from both oceans. Two major routes of the energy propagation are determined as a result of complex interplay of planetary waves within the archipelago. In the case of high frequency waves from the equatorial Pacific Ocean, most of their energy dissipate along the northern coast of New Guinea island outside of the archipelago. On the other hand, high frequency waves from the equatorial Indian Ocean are likely to reach the Pacific Ocean because of the existence of an additional pathway through the eastern side of the archipelago.

1 Introduction

The Indonesian throughflow (ITF), driven by the pressure gradient between the Pacific and Indian Oceans (Wyrski, 1987; Clarke & Liu, 1994), provides a low-latitude pathway of warm and fresh water from the Pacific to the Indian Ocean through the Indonesian archipelago (Gordon, 2005). The ITF constitutes a part of the global thermohaline circulation (Gordon, 1986; Sloyan & Rintoul, 2001), which controls global climate as well as regional and local climate over the Indonesian archipelago. The Indonesian seas also play a role as a wave path connecting the Pacific and the Indian Ocean, by which ocean and climate conditions within the Indonesian archipelago and the surrounding area are affected at various time scales.

Direct observations of the sea level and thermocline temperature variability within the Indonesian archipelago and southeastern Indian Ocean indicate that the interannual variability in these variables are associated with wind forcing in equatorial Pacific, suggesting oceanic wave propagation from the equatorial Pacific to the Indian Ocean through the Indonesian archipelago (Wijffels & Meyers, 2004). Another study by J. Li and Clarke

(2004) using sea level observations also shows penetration of the El Niño signal into the Indonesian archipelago and further into the north and west coast of Australia. Due to the influence of these ocean waves propagating from the Pacific Ocean, the ITF transport and downstream Leeuwin Current show significant variability including the El Niño related signals (Gordon et al., 1999; Feng et al., 2003). It is also suggested that the ocean waves from the Pacific Ocean may generate the Ningaloo Niño events appeared along the northwestern coast of Australia (Kataoka et al., 2014).

The Indonesian archipelago can also be considered as incomplete boundaries of the two basins. Reflection of the equatorial Rossby waves at the entrance of the Indonesian archipelago has been extensively studied as an important process in the delayed action oscillator theory of the El Niño-Southern Oscillation (ENSO) (Suarez & Schopf, 1988). There are several theoretical studies investigating impacts of the reflection of equatorial waves at the leaky Pacific western boundary on the signal reaching the Indian Ocean, which is dynamically associated with the ENSO phenomenon (Clarke, 1991; Du Penhoat & Cane, 1991). In particular, Clarke (1991) assumes the land masses in the western Pacific Ocean and the Indonesian archipelago as thin meridional walls located at representative longitude of each island and suggests that 10% of the energy of the meridional mode 1 Rossby wave coming from the equatorial Pacific penetrates into the Indian Ocean through the Indonesian archipelago at interannual timescales.

To estimate a degree of wave reflection and signal penetration quantitatively with the realistic geometry in the archipelago, reduced gravity models are frequently utilized in several previous studies. Potemra (2001) suggests that energy from the central equatorial Pacific does affect not only the ITF transport but also variability in the southeastern Indian Ocean with significant amplitude at semiannual and longer time scales. Further numerical study by Spall and Pedlosky (2005) shows that 23% of the energy from the equatorial Rossby wave is reflected into the equatorial Kelvin wave at the leaky western boundary of the Pacific Ocean and 10% of the energy reaching the Indian Ocean.

In addition, many studies suggest that significant non-ENSO signals in the ITF transport come from the tropical Indian Ocean (Murtugudde et al., 1998; Qiu et al., 1999; Sprintall et al., 2000; Molcard et al., 2001). For example, Sprintall et al. (2000) observed that a semiannual Kelvin wave, excited in the equatorial Indian Ocean, propagates southeastward along the Sumatra/Java coasts, through the Lombok Strait, and then northward to the Makassar Strait. In addition to the Lombok Strait, the Ombai Strait is also suggested to be an important pathway for the coastally trapped Kelvin waves originated from the equatorial Indian Ocean to flow into the Indonesian archipelago (Durland & Qiu, 2003; Wijffels & Meyers, 2004; Syamsudin et al., 2004). Furthermore, the simple model experiments of Yuan et al. (2018) suggest the possibility of Kelvin wave penetration into the western Pacific from the eastern Indian Ocean through both eastern and western parts of the Indonesian archipelago.

Even if we focus on the horizontal propagation of linear waves, the behavior of the incoming waves with intraseasonal time scale within the Indonesian archipelago is not well understood. Moreover, there is a lack of discussions about where the energy dissipation occurs and how it affects the wave transmission through the archipelago in case of the intrusion of equatorial waves. Therefore, to improve our understanding of processes responsible for the bulk effect of the archipelago, we focus on the incoming waves with a wide range of periodic bands including intraseasonal waves, and the energy dissipation associated with wave propagation.

Recently, Aiki et al. (2017) develops a new analysis scheme of wave energy flux for the planetary waves, which can be applied seamlessly in terms of the latitudinal region. In the present study, therefore, we also examine detailed pathways of wave propagation both from the Pacific to Indian Oceans, and vice versa, by quantitative evaluation based on the wave energy flux of Aiki et al. (2017). For these purposes, a simple reduced grav-

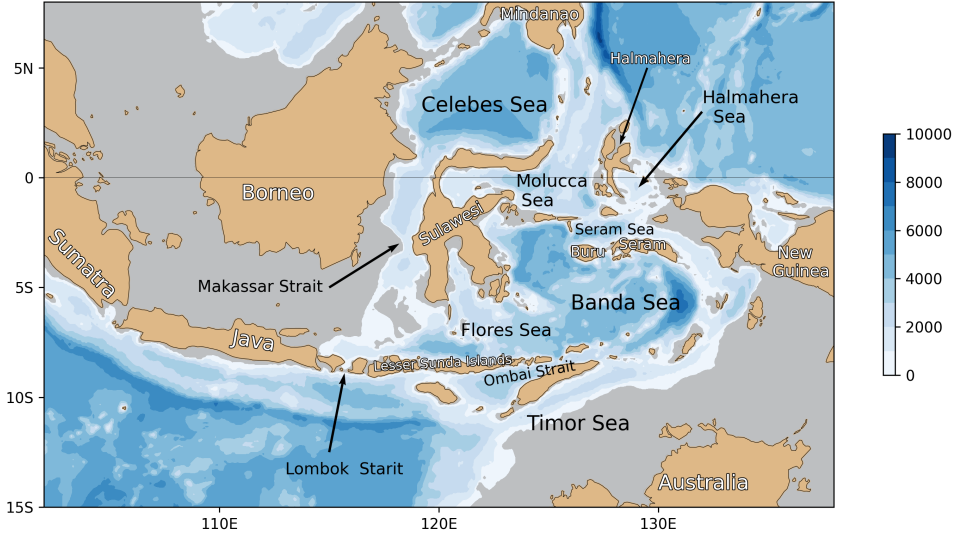


Figure 1. Topography in the Indonesian archipelago. Depths are given in meter. Gray shades indicate areas with depth shallower than 300 meters, which is considered as land masses in the reduced gravity model used in this study.

117 ity model with realistic representation of the complex geometry of the Indonesian archipelago
 118 (Fig. 1) is adopted.

119 This paper is organized as follows. A numerical model and a method to calculate
 120 the wave energy flux are described in Section 2. Section 3 shows results for the cases,
 121 in which waves come from the equatorial Pacific Ocean. The wave energy pathways in
 122 the Indonesian archipelago and their dependences are discussed. Results for incoming
 123 waves from the equatorial Indian Ocean are described in Section 4. Summary and dis-
 124 cussion are presented in Section 5.

125 2 Model and Method

126 2.1 Numerical Model

127 We adopt a linear reduced gravity model with one active layer to explore paths of
 128 wave energy exchange between the eastern Indian and western Pacific Oceans through
 129 the Indonesian archipelago in the simplest possible system. The equations for this model
 130 are written as:

$$\begin{aligned} \frac{\partial u}{\partial t} - yv + \frac{\partial p}{\partial x} &= 0 \\ \frac{\partial v}{\partial t} + yu + \frac{\partial p}{\partial y} &= 0 \\ \frac{\partial p}{\partial t} + \frac{\partial u}{\partial x} + \frac{\partial v}{\partial y} &= 0 \end{aligned}$$

131 where u and v are zonal and meridional velocities, respectively, η is upper layer thick-
 132 ness anomaly, f is the Coriolis parameter, g' is the reduced gravity and τ_x and τ_y cor-
 133 respond to zonal and meridional wind stress, with $\tau_y = 0$ for all the experiments in this
 134 study. The mean thickness of the active upper layer H is set to 300 m, and the coeffi-
 135 cient of horizontal viscosity ν has a value of $1 \times 10^{-3} \text{ m}^2 \text{ s}^{-1}$. The model has a realis-
 136 tic land geometry in and around the Indonesian archipelago based on the contour of 300

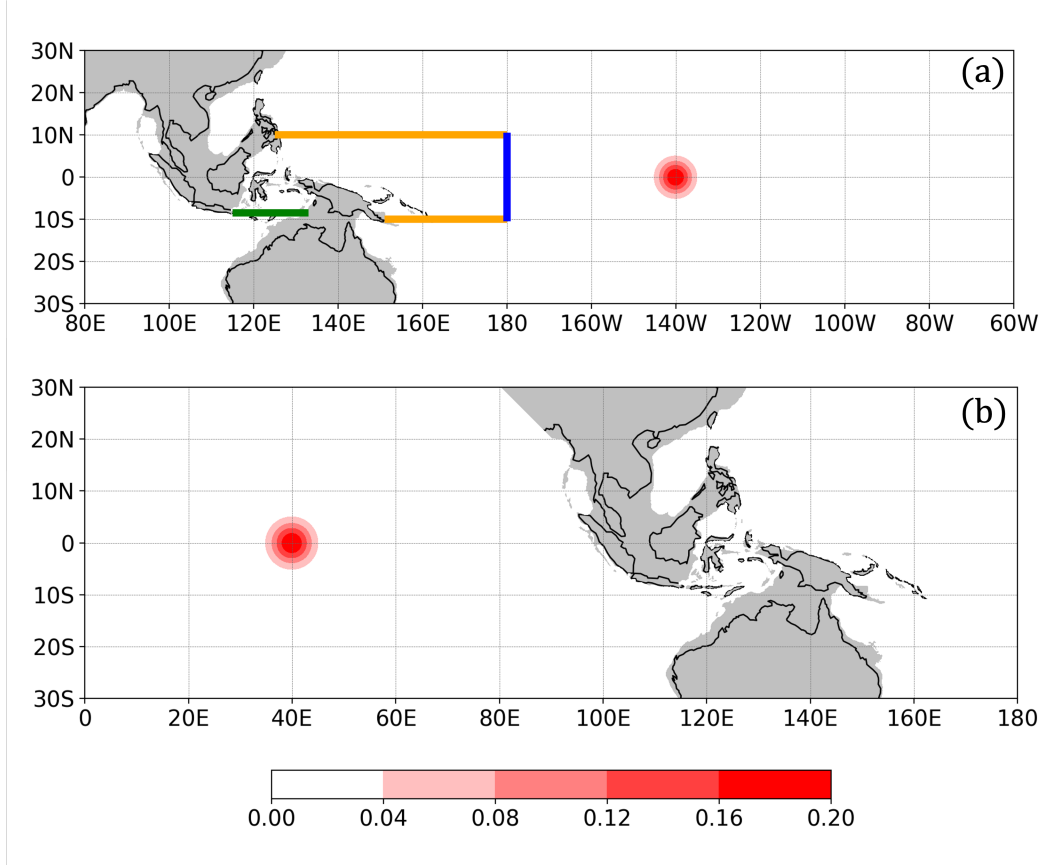


Figure 2. Model domains for (a) the Pacific Ocean experiment and (b) the Indian Ocean experiment, with the amplitude of the idealized zonal wind forcing in N m^{-2} (*color shading*). The model boundaries based on the 300 m isobaths (*gray shade*) are also shown.

137 m isobath from ETOPO1 (Amante & Eakins, 2009), and is forced by idealized zonal winds
 138 with a prescribed period of variation. This model is discretized into a spherical coordi-
 139 nate system with a grid spacing of 0.1° in both zonal and meridional directions on the
 140 Arakawa-C grid system. At each position of the respective variables, the model integrated
 141 the above equations for zonal velocity u , meridional velocity v and upper layer thickness
 142 anomaly η . The gravity wave speed $c = \sqrt{g'H}$ was set equal to $c = 2.62 \text{ m s}^{-1}$ as in
 143 Potemra (2001), assuming the first baroclinic mode waves in the equatorial Pacific Ocean.

144 A series of experiments is conducted with two model domains to focus on equatorial
 145 waves coming from the equatorial Pacific Ocean or from the equatorial Indian Ocean,
 146 respectively. For the Pacific experiment, the model domain extends from 80°E to 60°W
 147 and from 30°S to 30°N (Fig. 2a). Sponge layers with the zonal width of 10 degrees for
 148 the artificial meridional boundaries at 80°E and 60°W and the meridional width of 5 de-
 149 grees for the zonal boundaries at 30°S and 30°N are applied along the artificial bound-
 150 aries to absorb the wave energy and eliminate unexpected reflection and propagation of
 151 the waves along the artificial boundaries. Note that results shown below are robust with
 152 a wider model domain to include the whole Indian Ocean, since the energy absorption
 153 within the sponge layer is quite effective.

154 Idealized wind forcing for the Pacific experiment is given as

$$\tau_x = A_0 \sin(\omega t) \exp \left[- \left(\frac{x - x_0}{L_x} \right)^2 - \left(\frac{y - y_0}{L_y} \right)^2 \right]$$

155 where (x_0, y_0) is at 140°W on the equator, L_x and L_y are zonal and meridional widths,
 156 respectively, with 4 degrees in both directions, A_0 is forcing amplitude of 0.2 N m^{-2} , and
 157 ω is the forcing frequency. Since the meridional decay scale L_y is larger than the equa-
 158 torial deformation radius ($\sim 330 \text{ km}$), it is expected that the Rossby wave of the first
 159 meridional mode is mainly excited (Spall & Pedlosky, 2005). We apply various forcing
 160 period from 90 days to 10 years in this study. The model is integrated for 10 forcing cy-
 161 cles, and the last cycle of the forcing period is used for the following analyses.

162 The Indian experiment is set similar to the Pacific experiment, but the domain ex-
 163 tends from 0° to 180° and from 30°S to 30°N (Fig. 2b). The gravity wave speed c is given
 164 as 2.99 m s^{-1} for the first baroclinic mode used in Z. Li and Aiki (2020), and wind stress
 165 is applied as

$$\tau_x = A_1 \sin(\omega t) \exp \left[- \left(\frac{x - x_1}{L_x} \right)^2 - \left(\frac{y - y_1}{L_y} \right)^2 \right]$$

166 where (x_1, y_1) is at 40°E on the equator. For the Indian Ocean experiment, we adopt
 167 the forcing period from 10 days to 4 years. The other parameters and settings are the
 168 same as in the Pacific experiment.

169 2.2 Analysis Method

170 Energy flux associated with planetary scale waves is a good indicator for pathways
 171 of the wave signals connecting the two basins through the Indonesian archipelago. To
 172 obtain wave energy flux in the above numerical model, We utilize a new formulation pro-
 173 posed by Aiki et al. (2017) (hereafter AGC17 scheme), which can be applicable at all lat-
 174 itudes, including the equatorial region, while satisfying coastal boundary conditions. See
 175 Appendix for derivation and detailed explanation of the formula. Note that the AGC17
 176 scheme can represent the wave propagation even in the regions where the contribution
 177 of viscosity term is large, such as the Indonesian archipelago.

178 3 Rossby waves from the Pacific to the Indian Oceans

179 3.1 Energy flux pathways

180 First, we examine results from experiments with wind forcing in the Pacific Ocean
 181 to see the pathways of wave energy transmitted through the Indonesian archipelago. The
 182 outputs from the reduced gravity model clearly shows that the wind forcing centering
 183 at 140°W excites westward propagating equatorial Rossby waves and eastward propa-
 184 gating equatorial Kelvin waves (Fig. 3a).

185 The maximum amplitude of the sea level anomaly associated with these equato-
 186 rial waves is about 5 cm, which is consistent with the satellite observations (Busalacchi
 187 et al., 1994; Boulanger & Menkes, 1995; Boulanger & Fu, 1996; Boulanger & Menkès,
 188 1999). Zonal energy flux along the equator clearly shows the eastward propagation of
 189 the equatorial Kelvin waves and the westward propagation of the equatorial Rossby waves (Fig.
 190 3b). Meridional distributions of the zonal energy flux across the international date line
 191 from the experiments with the forcing of 4-year and semiannual periods are shown in the
 192 boxes on the right side of Fig. 4. The meridional structure of the energy flux indicates
 193 that almost all incoming waves are meridional mode 1 Rossby waves as expected from
 194 the model results of Spall and Pedlosky (2005). Moreover, the horizontal distributions
 195 of the wave energy fluxes (left panels in Fig. 4) show the signals penetrating from the

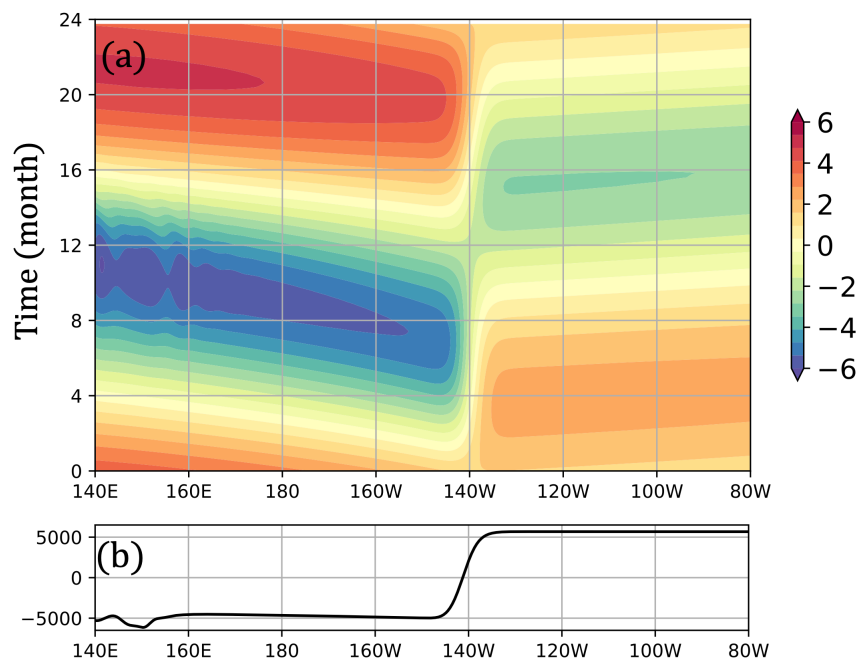


Figure 3. (a) Hovmoller diagram of the sea level anomaly along 2°N for the 2-year period forcing case. The unit is cm. (b) Zonal component of energy flux along the equator for the 2-year period forcing case. The unit is W m^{-1} .

Table 1. Southward energy flux crossing the equator through each passage. Positive value indicates the wave energy flowing into the Indonesian archipelago with a unit of 10^9 W=1 GW.

Period(year)	Makassar St.	Molucca Sea	Halmahera Sea
0.5	0.15	-0.22	0.84
1	0.22	-0.29	0.85
2	0.24	-0.30	0.81
4	0.23	-0.31	0.82

Table 2. Wave energy flux into the Indian Ocean from the Indonesian seas through each passage with a unit of 10^9 W=1 GW.

Period(year)	Lombok St.	Ombai St.	Timor Sea
0.5	0.07	0.05	0.16
1	0.11	0.08	0.14
2	0.12	0.09	0.13
4	0.13	0.09	0.12

196 Pacific to the Indian Ocean, and then waves continue to propagate southward along the
 197 western coast of Australia. The maximum amplitude of the sea level along the western
 198 coast of Australia is about 3.5 cm, which is consistent with the observed sea level vari-
 199 ations (Clarke & Liu, 1994; Feng et al., 2003). Therefore, the present simple model and
 200 its results capture a realistic situation of ocean wave propagation and are worth inves-
 201 tigating the detailed processes.

202 *3.1.1 Interannual time-scale*

203 The left panels of Fig. 4 show horizontal distributions of energy flux vectors within
 204 and around the Indonesian archipelago, indicating very complex pathways of wave en-
 205 ergy from the Pacific to the Indian Oceans for the first time. Note that these vectors only
 206 indicate the direction of the energy fluxes and their magnitude is shown in color shades
 207 to see the pathways clearly. Table 1 and 2 summarize the energy flux through several
 208 key passages at the northern entrance and the southern exit for the archipelago.

209 In general, for the forcing period of interannual time-scales, most of the wave en-
 210 ergy propagates through the Indonesian archipelago within its eastern part; through the
 211 Halmahera Sea, the Banda Sea, and the Timor Sea, before reaching the northwestern
 212 coast of Australia (Fig. 4a). This eastern route of the wave energy pathway is consis-
 213 tent with the previously mentioned wave pathway suggested from the observed temper-
 214 ature variability and sea level data (e.g. Wijffels & Meyers, 2004). However, there can
 215 be seen several notable details in Fig. 4a, which have not mentioned in the previous lit-
 216 eratures. One such feature is that the major route of the wave energy occupies the west-
 217 ern side of island chain in the eastern Banda Sea. Considering the Kelvin wave propa-
 218 gation along the coasts in the southern hemisphere, major part of the energy flux would
 219 be expected through the passage between the Seram and New Guinea Islands. However,
 220 most of the energy propagates into the Banda Sea along the west coast of Buru Island
 221 and almost no energy propagates along the west coast of New Guinea. We will explore
 222 a possible reason for this curious wave energy flux distribution in the following subsec-
 223 tion.

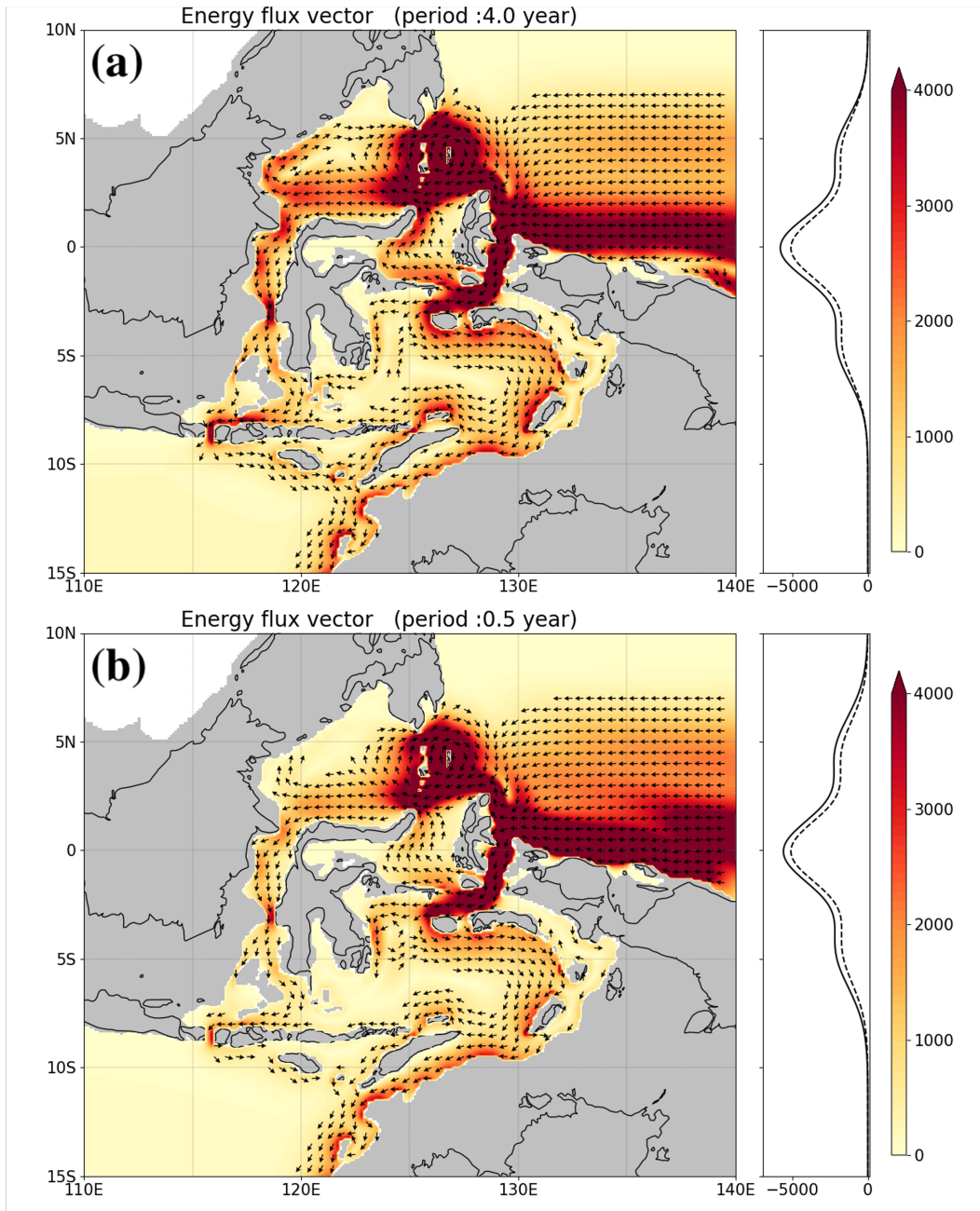


Figure 4. (Left panels) Horizontal distribution of the direction of energy flux vectors (*arrows*) and magnitude of the energy flux in W m^{-2} (*color*). The energy flux vectors are shown only for those with their magnitude larger than 400 W m^{-2} . (Right panels) Meridional distribution of the zonal energy flux of pure incoming wave energy (*solid line*) and analytical values for the first meridional mode 1 Rossby wave (*dashed line*) in W m^{-2} . The forcing period is (a) 4 years and (b) 0.5 years.

224 After reaching the southern part of the Banda Sea, most of this southward energy
 225 flux continue to the Indian Ocean via the Timor Sea. Note that theIn addition, weak
 226 southward energy flux appears along the east coast of Sulawesi Island within the Banda
 227 Sea from 3°S to 7°S. Note that this poleward energy flux along the east coast of Sulawesi
 228 Island is in the opposite direction to the energy propagation due to the coastal Kelvin
 229 wave in the southern hemisphere. It is suggested, therefore, that this poleward energy
 230 flux is associated with the diffusive boundary layer as mentioned in Spall and Pedlosky
 231 (2005). In fact, the width of the southward energy flux along the east coast of Sulawesi
 232 Island in the simulated result is about 80 km at 4°S, which is consistent with the rep-
 233 resentative width of diffusive boundary layer with the viscosity coefficient of $1 \times 10^3 \text{ m}^2$
 234 s^{-1} .

235 A part of the energy coming to the region south of Halmahera Island returns north-
 236 ward through the Molucca Sea (Table 1), then it merges to the westward energy flux from
 237 the northern tip of Halmahera Island to form rather broad westward energy flux to the
 238 north of Sulawesi Island. Fig. 4a also shows that about 60% of this wave energy flows
 239 into the Makassar Strait and then reaches the Lombok Strait. Besides, the remaining
 240 40% of the wave energy propagates northward along the eastern coast of Borneo Island.
 241 This poleward energy propagation is not consistent with the propagation of coastal Kelvin
 242 wave, and width of the northward energy flux is about 100 km, suggesting again the en-
 243 ergy redistribution in the diffusive boundary layer similar to the eastern coast of Sulawesi
 244 Island. It is suggested that not only the wave energy from the Makassar Strait but also
 245 the wave energy from the Halmahera Sea and the Banda Sea proceed to the Lombok Strait.
 246 Indeed Fig. 4a shows westward energy flux in the Flores Sea, which is due to the Rossby
 247 waves off the southern coast of Sulawesi and coastal Kelvin waves along the northern coast
 248 of the Lesser Sunda Islands.

249 Finally, most of the energy propagating southward in the Indonesian archipelago
 250 continue to the Indian Ocean mainly via the Timor Sea and Lombok Strait, with the re-
 251 maining southward energy transfer through the Ombai Strait (Table 2). Although the
 252 width of the Ombai Strait is relatively wide compared to the deformation radius at the
 253 location of the strait, it is the westward energy fluxes in the Flores Sea that transport
 254 a part of energy to the Lombok Strait. Note that the same wave energy pathways as de-
 255 scribed above are reproduced in experiments with a horizontal viscosity of $1 \times 10^2 \text{ m}^2$
 256 s^{-1} , i.e. ten times larger than the standard case.

257 In addition, since recent mooring observation suggests that the wave propagation
 258 through the Halmahera Sea is not as remarkable as that assumed to be a major wave-
 259 guide in previous studies (X. Li et al., 2020), the Halmahera Sea in the model of this study
 260 may be more favorable to wave transmission due to insufficient resolution ($\sim 10 \text{ km}$) to
 261 represent many small islands in the Halmahera Sea. However, there is no change in the
 262 wave energy pathway in the experiment which applied high horizontal viscosity (5×10^3
 263 $\text{m}^2 \text{ s}^{-1}$) only in the Halmahera Sea.

264 *3.1.2 Role of Halmahera Island and islands in Banda Sea on the en-* 265 *ergy pathways*

266 In the previous subsection, the importance of Halmahera Island and islands in Banda
 267 Sea on the pathways of wave energy impinging from the equatorial Pacific Ocean is sug-
 268 gested. Here we try to explore their roles in more details with additional experiments
 269 removing these islands in the model. In order to clarify the role of Halmahera Island,
 270 we first conduct simple experiment only with New Guinea and Australia, without Halma-
 271 hera Island, and with annual wind forcing as in the main experiments. Fig. 5a shows the
 272 energy fluxes in this experiment. It is clearly indicated that most of the incoming en-
 273 ergy continues to propagate westward and a small part of the energy propagates along
 274 the west coast of New Guinea as coastal Kelvin wave. Slight westward energy fluxes, shown

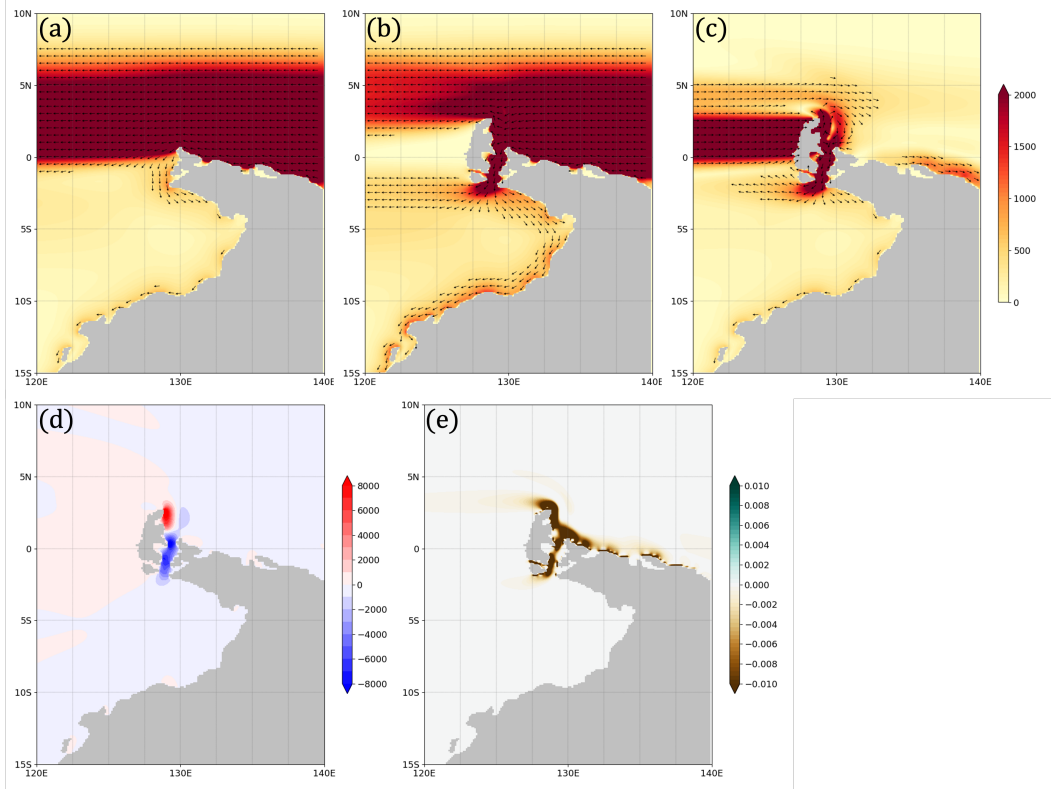


Figure 5. Horizontal distributions of (a) energy flux from a sensitivity experiment only with New Guinea and Australia, (b) energy flux from a sensitivity experiment to which Halmahera Island is added and (c) energy flux differences between the two sensitivity experiments. Arrows indicate energy flux vectors with magnitude larger than 400 W m^{-1} and red color shading indicates magnitude of energy flux in W m^{-1} . (d) Horizontal distribution of the meridional component of energy flux differences in W m^{-1} . (e) Horizontal distribution of the viscous dissipation near Halmahera Island and New Guinea for with Halmahera case in W m^{-1} .

275 as light color shades without arrows, corresponding to Rossby wave emitted from the coastal
 276 Kelvin wave can also be seen on the western side of New Guinea and Australia.

277 As a second step, Halmahera Island is added to the experiment (Fig. 5b). The dif-
 278 ference in the energy flux between the two experiments (Fig. 5c,d) can be considered as
 279 the contribution of Halmahera Island to the wave energy propagation. Fig. 5c clearly
 280 shows that the Halmahera Island has a barrier effect on the westward equatorial Rossby
 281 wave, and the blocked Rossby wave energy continues to propagate southward through
 282 the Halmahera Sea, resulting in enhancement of the Rossby waves in southern hemisphere
 283 and the southward coastal Kelvin wave. Fig. 5d shows strong southward and northward
 284 energy fluxes in the Halmahera Sea, and strong energy dissipation along the eastern coast
 285 of the Halmahera Island is shown in Fig. 5e. All these results suggest the importance
 286 of the diffusive boundary layer to the wave energy propagation.

287 To investigate the reasons why the wave energy does not propagate along the west
 288 coast of New Guinea as shown in Fig. 4, we conducted an additional sensitivity exper-
 289 iment with Buru and Seram Islands and the island chain in the eastern Banda Sea. Fig.
 290 6 shows the contribution of these islands to the energy transport. The island chain has
 291 only a small effect on wave energy to reflect back to the Pacific Ocean, and most of the

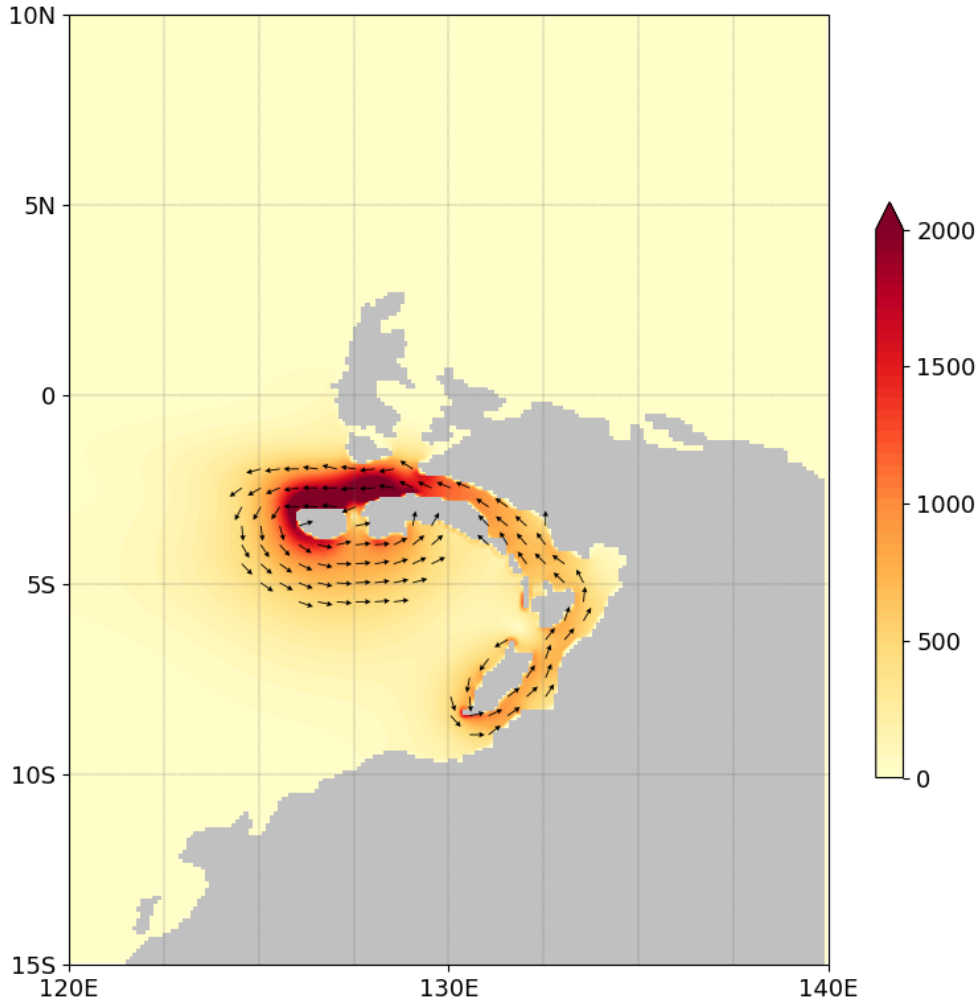


Figure 6. Same as Fig. 5c but for the energy flux differences between experiments with and without Buru and Seram Islands and the island chain in the eastern Banda Sea. (with island chain case minus no island chain case)

292 wave energy flows into the Indian Ocean as in the case with Halmahera Island (Fig. 5b).
 293 In addition, an anticlockwise energy circulation around the island chain is clearly seen
 294 in Fig. 6, which is superposed on the southward energy flux along the west coast of New
 295 Guinea in the case with Halmahera Island, providing almost no energy flux in the total
 296 fields. Thus, the absence of the easternmost energy path can be attributed to the cancellation
 297 of Kelvin wave along the west coast of New Guinea by the energy circulation
 298 trapped around the islands in the Banda Sea. It takes only about 10 days for Kelvin waves
 299 to bypass the islands of the Banda Sea and develop the energy circulation with the group
 300 velocity of the first baroclinic mode coastal Kelvin wave ($\sim 2.6 \text{ m s}^{-1}$), suggesting that
 301 it is difficult to detect signals that has a period longer than 10 days from the Pacific Ocean
 302 using mooring observations on the west coast of New Guinea.

3.1.3 Semiannual time-scale

The energy pathways shown for the incident waves of different interannual time scales (2- to 10-year period) are very similar to those obtained for the 4-year period case discussed above. The approach taken in this study, numerical experiments with realistic boundaries and AGC17 scheme, also enables us to investigate the energy propagation of higher frequency waves, which has not been discussed much in the previous literatures. It is important to evaluate energy pathways for such shorter time-scale variations since the semiannual variations are observed in the western tropical Pacific (e.g. Qu et al., 2008). In addition, atmospheric intraseasonal oscillations, such as the Madden-Julian oscillation (Madden & Julian, 1994), can generate equatorial Kelvin and Rossby waves through surface zonal winds over the Pacific Ocean (Hendon et al., 1998; Zhang et al., 2001) and may affect the Indonesian archipelago.

The results of semi-annual forcing case (Fig. 4b) also show two major energy pathways; one through Halmahera Sea and Banda Sea and the other through Makassar Strait and Lombok Strait as in the case of low frequencies. However, the magnitude of the energy flux is clearly smaller than that of the low frequency case. In particular, the decrease in magnitude is significant in the pathway through the Makassar Strait and Lombok Strait (see Table 2). This discrepancy is attributed to the difference in the amount of energy dissipation at the western boundary of the Pacific Ocean, which is discussed in the next subsection on the energy budget. The decrease in the energy flux through the Lombok Strait may also be due to the reduction of the westward propagating Rossby wave in the Flores and Banda Seas at high frequencies.

3.2 Energy budget

3.2.1 Energy budget for a larger domain

To evaluate the energy budget in a larger domain, a box covering the western equatorial Pacific and the Indonesian archipelago is considered (Fig. 2a) and the amount of wave energy crossing the boundaries is calculated (Fig. 7). It should be noted here that wave energy flux across the eastern section at 180°E averaged over one forcing period, E'_{in} includes both the incoming wave energy flux and the flux due to reflected waves. In order to extract pure incoming wave energy crossing the international date line, we conducted an additional experiment, in which a simple meridional western boundary with a sponge layer is incorporated to erase the wave energy associated with the reflected equatorial Kelvin wave. The energy flux across the international date line for this experiment can be considered as the pure westward incoming wave energy, E_{in} , and therefore eastward reflected wave energy, E_{ref} , can be defined as

$$E_{\text{ref}} = E_{\text{in}} - E'_{\text{in}}$$

Fig. 7 shows results of the energy budget as a function of the forcing period, standardized by the incoming energy across the date line for each forcing period. It is clearly shown that, for the period longer than 1.5 years, most of the incoming energy (about 60%) is dissipated within the box, while about 30% of the incoming energy is reflected back to the east of the date line. Then, the remaining 10% of the incoming energy flows into the Indian Ocean. Since the wind forcing in our experiment excites the meridional mode 1 equatorial Rossby wave (see Fig. 4), this result is in good agreement with the result of the analytical investigation by Clarke (1991) and the model calculations by Spall and Pedlosky (2005).

Horizontal distributions of energy dissipation rate are shown in Fig. 8. Comparing high frequency and low frequency cases, there is a common feature that strong energy dissipation occurs in the western boundary layer regions of the Pacific Ocean, such as zonally narrow regions off the east coast of Mindanao, Borneo, Halmahera and New

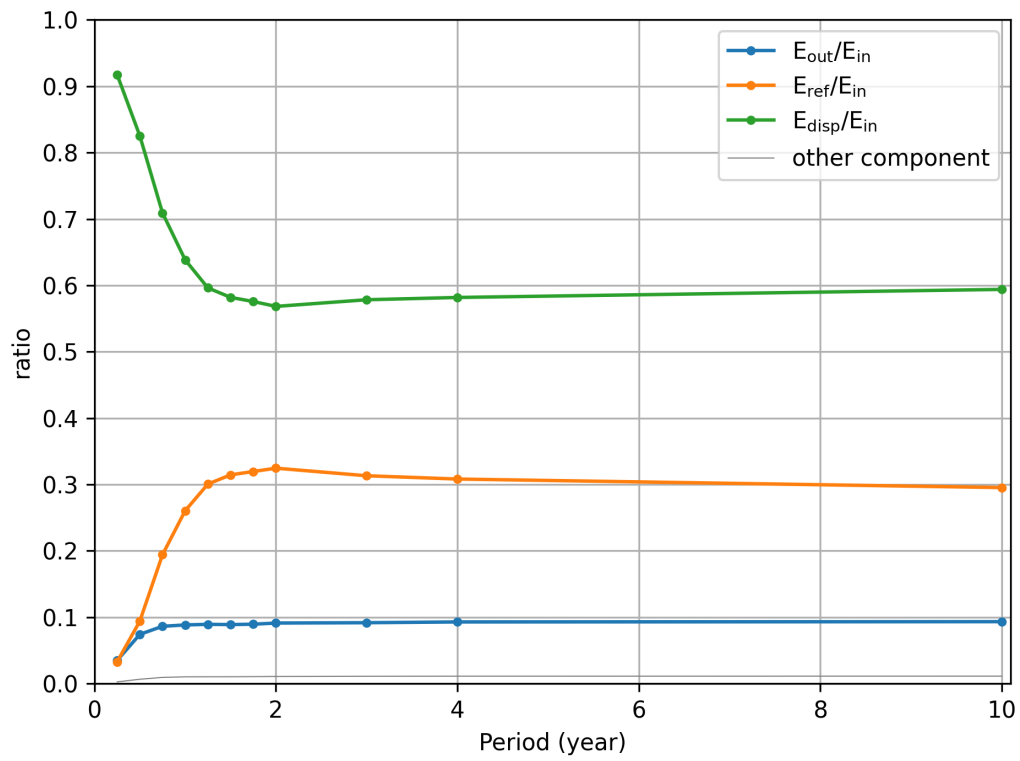


Figure 7. Ratios of major terms in the wave energy budget in the box shown in Fig. 2a to the pure incoming wave energy flux across the international date line.

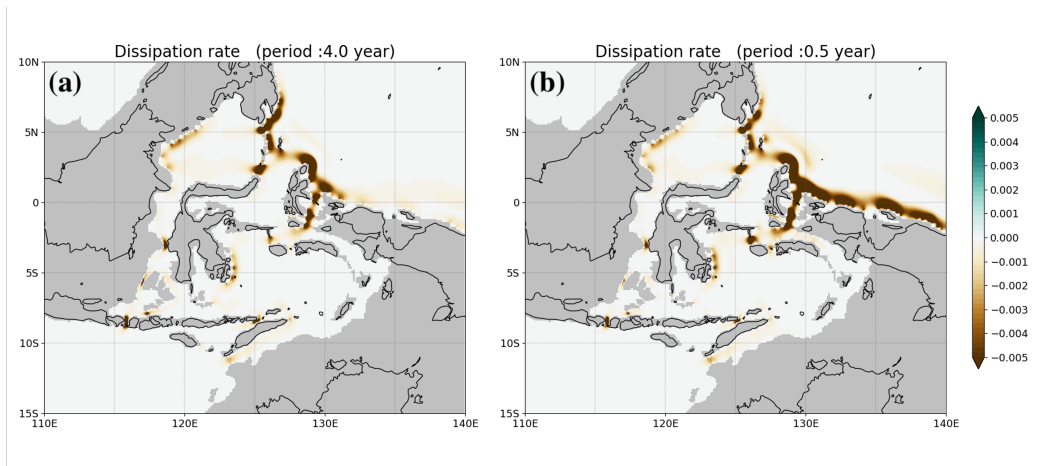


Figure 8. Horizontal distribution of dissipation rate obtained from experiments with the wind forcing of (a) 4 year and (b) 180 day periods. The unit is W m^{-2} .

351 Guinea, as well as regions within the narrow channel such as the Halmahera Sea and the
 352 northern entrance of the Banda Sea. In addition, there is strong energy dissipation in
 353 the northern coast of Buru Island, as well as the narrow part of the Makassar Strait and
 354 the Lombok Strait. Note that northward and southward leakage of the energy across 10°N
 355 and 10°S are almost negligible for all frequencies.

356 For the forcing period less than 1.5 years, unlike the low frequency case, the ratio
 357 of dissipated energy within the box increases and that of reflected energy decreases as
 358 the period becomes shorter (Fig. 7). This tendency is consistent with the result of Spall
 359 and Pedlosky (2005), but their result only shows the decreases of dissipated and trans-
 360 mitted energy qualitatively. Thus, detailed quantitative understanding of why the re-
 361 flection and the transmission are suppressed at higher frequency is necessary. In the high
 362 frequency case (Fig. 8b), the dissipation rate is significantly large along the northern coast
 363 of New Guinea between 130°E and 140°E , which cannot be seen in the low frequency
 364 case (Fig. 8a). The forcing period of 1.5-year seems to provide a key time-scale for set-
 365 ting up two regimes; one with the weaker dissipation along the northern coast of New
 366 Guinea (i.e. the low-frequency cases) and the other with the stronger dissipation there
 367 (i.e. the high-frequency cases). It is worth noting that the 1.5-year corresponds to a wave
 368 period, for which half of the zonal wavelength of the incoming meridional mode 1 Rossby
 369 wave is comparable to the zonal width of the inclined western boundary (New Guinea
 370 Island) in the present case. We will discuss a possible mechanism responsible for this dif-
 371 ference in the dissipation magnitude in detail in the next subsection.

372 *3.2.2 Dissipation along the northern coast of New Guinea*

373 In the previous studies of the reflection of the equatorial Rossby waves at inclined
 374 western boundary (e.g. Cane & Gent, 1984; McCalpin, 1987), the reflection at the west-
 375 ern boundary is considered from the budget of mass flux across the boundary between
 376 the western boundary layer and the interior ocean, and remaining energy is treated to
 377 be dissipated in the western boundary layer. However, since we consider the energy pen-
 378 etration further to the west, we need to examine the energy dissipation on the inclined
 379 western boundary in detail.

380 To evaluate the energy dissipation on the western boundary in a simpler case, ex-
 381 periments without Solomon Islands and New Ireland are conducted. In these additional

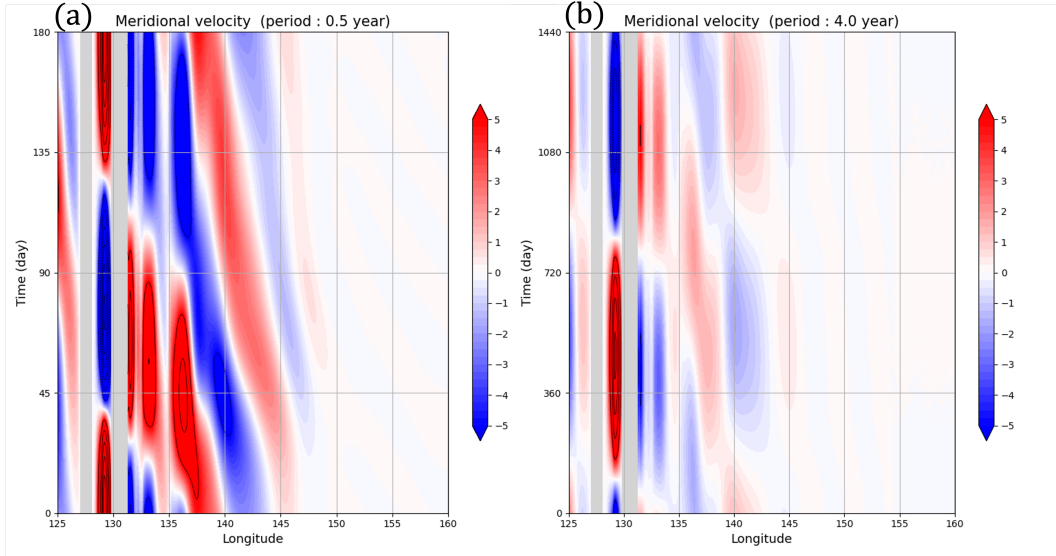


Figure 9. Hovmöller diagrams of the meridional current along the equator for (a) the 4-year period forcing case and (b) the semi-annual forcing case in cm s^{-1} . Contours indicate meridional velocity with amplitudes above 5 cm s^{-1} and contour intervals are 5 cm s^{-1} .

382 experiments, energy transmission and reflection rates show the same dependencies on
 383 the forcing period as in the main experiments (Fig. 7). Furthermore, strong energy dis-
 384 sipation along the northern coast of New Guinea can be seen only when forcing period
 385 is shorter than 1.5 years. Fig. 9 shows time evolutions of meridional currents along the
 386 equator when the forcing periods are 4 years and 0.5 years. In both cases, the meridional
 387 velocity is significant in the region near the western boundary of the Pacific Ocean (130-
 388 145°E). However, the amplitudes of the meridional velocity show very different values:
 389 it is about 2 cm s^{-1} for the 4-year period case while it becomes well over 5 cm s^{-1} for
 390 the 0.5-year period case.

391 To clarify the processes that generate the meridional currents across the equator
 392 with different amplitude for the short-period and long-period cases, we consider the mass
 393 flux entering the inclined west boundary layer as in Cane and Gent (1984); McCalpin
 394 (1987). When the forcing period is long enough (the zonal wavelength of the incoming
 395 Rossby waves is sufficiently longer than the zonal extent of the inclined western bound-
 396 ary), incoming Rossby waves reach the western boundary layer at almost the same phase
 397 at any latitude, and the meridionally symmetric mass fluxes enter the west boundary layer.
 398 In this case, most of the off-equatorial incoming mass fluxes of the Rossby waves gener-
 399 ate equatorward currents in the western boundary layer for redistributing the masses
 400 toward the equator and emitting them eastward as the equatorial Kelvin waves. The di-
 401 rection of the mass redistribution in the western boundary layer is opposite in the north-
 402 ern and southern hemispheres, thus meridional current across the equator is less likely
 403 to be formed (Fig. 9a). On the other hand, when the forcing period is rather short, i.e.
 404 the zonal wavelength of the incoming Rossby waves is comparable to or less than the zonal
 405 extent of the inclined western boundary, incoming Rossby waves reach the western bound-
 406 ary layer at different phases at each latitude, and the meridionally asymmetric mass fluxes
 407 are generated in the west boundary layer. For example, a positive mass flux enters in
 408 the southern hemisphere while a negative mass flux enters in the northern hemisphere.
 409 In this case, the total mass flux entering the western boundary layer, capable of construct-
 410 ing the reflected Kelvin waves, is very small. Therefore, strong meridional current across

411 the equator is formed to connect the asymmetric mass distribution in the western bound-
 412 ary layer (Fig. 9b). This strong current across the equator and in the western bound-
 413 ary layer generates large horizontal velocity shier, inducing the strong energy dissipa-
 414 tion particularly along the northern coast of New Guinea (Fig. 8b).

415 Since both the incoming meridional mode 1 Rossby waves and the reflected equa-
 416 torial Kelvin waves have no meridional velocity at the equator, the meridional currents
 417 shown in Fig 9 suggest the existence of the other type of waves. In fact, Fig. 9 indicates
 418 the westward phase speed of about 10 cm s^{-1} with the eastward group velocity of about
 419 50 cm s^{-1} between 140°E and 150°E , and this group velocity correspond to that of the
 420 Yanai waves with a period of about 20 days. The existence of the Yanai waves is also
 421 confirmed in Fig. 10, which shows the zonal distribution of the time averaged meridional
 422 velocity for the gravest four modes of the equatorial Rossby waves and the Yanai wave.
 423 When incident Rossby wave approaches the inclined western boundary, the meridion-
 424 ally asymmetric mode Rossby waves and the Yanai waves are excited to satisfy the bound-
 425 ary condition. Since these reflected waves have a group velocity smaller than the incom-
 426 ing meridional mode 1 Rossby waves, they are superposed on the incoming waves with
 427 the out-of-phase relation. Since the New Guinea coast extends far eastward to 150°E ,
 428 the superposition of the waves create a strong horizontal shear of the along shore cur-
 429 rent fields that efficiently dissipates wave energy. The proportion of time with strong hor-
 430 izontal current shear to one period of the incident Rossby wave becomes longer as the
 431 wavelength of the incident wave becomes shorter. Therefore, more energy is dissipated
 432 in the western boundary layer along the northern boundary of New Guinea when incom-
 433 ing wave period is shorter.

434 4 Kelvin Waves From the Indian to the Pacific Oceans

435 4.1 Responses within the Indian Ocean

436 For the Indian Ocean experiment, we consider whether and how the equatorial Kelvin
 437 waves propagate through the Indonesian archipelago and eventually penetrate into the
 438 Pacific Ocean. We first investigate briefly the behavior of waves before they reach the
 439 Indonesian archipelago. For a period shorter than 30.7 days, below which no equatorial
 440 Rossby waves satisfy the dispersion relation under our model settings, most of the wave
 441 energy propagates southeastward along the coast of Sumatra Island after reaching the
 442 eastern boundary of the Indian Ocean (Fig. 11a). Only a small part of the incoming wave
 443 energy propagates to the north into the Andaman Sea along the eastern boundary of the
 444 basin.

445 On the other hand, for the Kelvin waves with longer periods, the wave energy bi-
 446 furcates northward and southward off Sumatra Island. While most of the energy reflects
 447 westward as Rossby waves and propagates along the coast of the Bay of Bengal in the
 448 northern hemisphere, they are divided into westward Rossby waves and eastward coastal
 449 Kelvin waves in the southern hemisphere (Fig. 11b). Fig. 11c shows northward energy
 450 fluxes across 4° and 12° latitude sections near the eastern boundary in both hemispheres
 451 as a function of the forcing period. The results indicate that more than a half of the en-
 452 ergy crossing 4°N reaches 12°N and propagate further north into the Bay of Bengal while
 453 the energy reaching 12°S is almost zero. This north-south difference suggests that the
 454 Bay of Bengal is more sensitive to equatorial waves originating from the equatorial In-
 455 dian Ocean than the Southeastern Indian Ocean.

456 Fig. 11c also shows dependences of energy flux magnitude on the forcing period.
 457 While the wave energy across 4°N or 4°S is evenly distributed for the longer periods, we
 458 can find asymmetric energy partition between the two hemispheres for sufficiently short
 459 period, with more energy in the southern hemisphere. In addition, northward wave en-

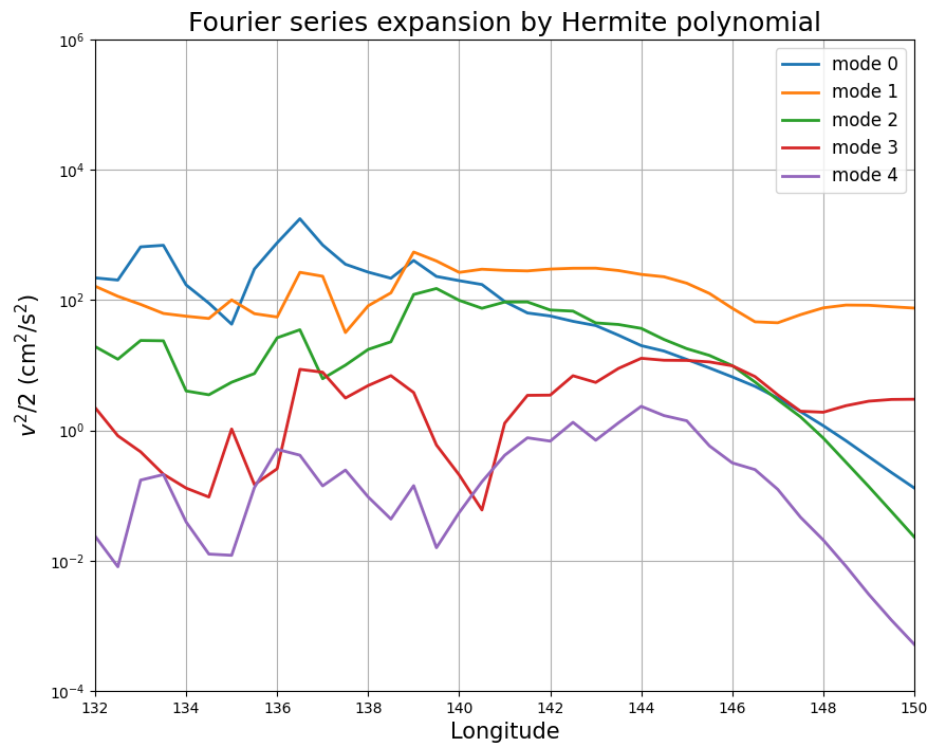


Figure 10. Time averaged amplitude of $v^2/2$ for each meridional mode of the equatorial waves for the semi-annual forcing case (Fourier series expansion by Hermitian function at each longitude). Mode 0 corresponds to the Yanai wave, while mode 1 to 4 indicates the Rossby waves with respective meridional structure.

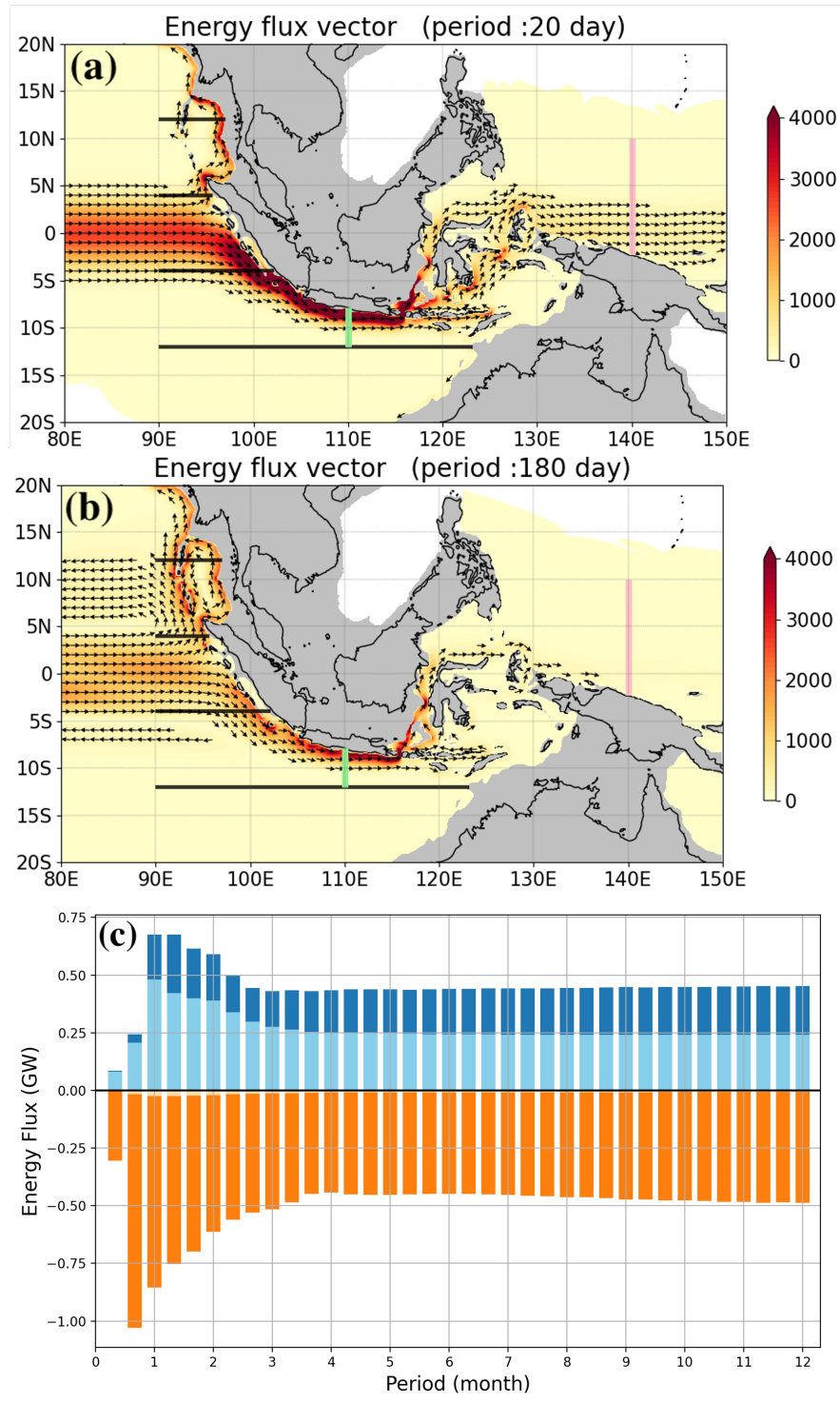


Figure 11. Horizontal distributions of the direction of energy flux vectors and magnitude of the energy flux for the forcing period of (a) 20 days and (b) 180 days. Only the vectors with their magnitude larger than $200 W m^{-1}$ are shown. (c) Northward energy fluxes across $4^{\circ}N$ (blue), $4^{\circ}S$ (orange), $12^{\circ}N$ (light blue) and $12^{\circ}S$ (pale orange) between $90^{\circ}E$ and the eastern boundary coast of the Indian Ocean for each forcing period. The sections calculating the energy fluxes are shown with black lines. Negative values indicate southward energy fluxes.

460 ergy across 4°N peaks at about a period of one month, consistent with the observed short-
 461 period westward-propagating Rossby waves near 5°N (Chen et al., 2017).

462 Unlike the low frequency case, when the high frequency Kelvin wave excited in the
 463 equatorial Indian Ocean reaches the eastern boundary, more energy is distributed to the
 464 south, and the distribution ratio to the south increases with reduction of the frequency.
 465 This asymmetric characteristic of the north-south distribution for the short wavelength
 466 waves may be caused by the absence of westward reflecting Rossby waves at high fre-
 467 quencies (Fig. 11a) and also affected by the inclination of the eastern boundary of the
 468 Indian Ocean from the north-south direction. This result suggests that when high fre-
 469 quency Kelvin wave reaches the inclined eastern boundary, more wave energy is distributed
 470 to the side where the boundary extends further east.

471 4.2 Energy flux pathways within the archipelago

472 The wave energy flux vectors in the Indonesian archipelago for the Indian exper-
 473 iments are shown in Fig. 12. An important common feature in all the results of these
 474 experiments with various forcing periods is that most of the incident energy enters the
 475 Indonesian archipelago through the Lombok Strait and then, flows into the western Pa-
 476 cific via the Makassar Strait. This waveguide is consistent with the route of wave sig-
 477 nal predicted by Clarke and Liu (1994), suggested from observed data by Sprintall et al.
 478 (2000) and Pujiana et al. (2013), for example, and simulated in numerical models of Syamsudin
 479 et al. (2004), Schiller et al. (2010) and Yuan et al. (2018), for example. It is confirmed
 480 for the first time with direct estimation of the energy fluxes that the same routes can
 481 also be seen as the dominant energy pathways.

482 As in the case of the Pacific experiments, the results of Indian experiments demon-
 483 strate different characteristics between the low and high frequency cases. For the low fre-
 484 quency case, the Kelvin wave signals enter the Indonesian archipelago mainly via the Lom-
 485 bok Strait and slightly via the Ombai Strait. The energy entered the Indonesian seas via
 486 the Ombai Strait propagates westward along the northern coasts of the Lesser Sunda Is-
 487 lands around 8°S and merges with energy from Lombok Strait (see Fig. 12c).

488 On the other hand, in the high frequency case, there appears a new route passing
 489 through the Indonesian seas from the Lombok Strait to the Pacific Ocean. The wave en-
 490 ergy coming into the archipelago via the Lombok Strait tends to follow the northward
 491 wave guide through the Makassar Strait. However, in the high frequency case (Fig. 12a),
 492 a part of this northward energy separates from the northward waveguide and propagates
 493 northeastward along the coast of Sulawesi Island and through the Molucca or Halma-
 494 hera Seas to reach the Pacific Ocean. The energy fluxes along this additional waveguide
 495 decrease with increasing period, probably due to excitation of the Rossby waves, which
 496 transport the energy westward in the Flores Sea to the Makassar Strait at sufficiently
 497 long period. In addition, the westward energy propagation from the Ombai Strait is not
 498 as strong as the low frequency case, although the wave energy entering the Indonesian
 499 archipelago through the Ombai Strait is larger in the high frequency case compared to
 500 the low frequency case.

501 From the above results, two major wave energy pathways from the Indian to the
 502 Pacific Oceans can be found:

- 503 1. The wave propagates northward through the Lombok and Makassar Straits and
 504 then across the Celebes Sea to the Pacific Ocean,
- 505 2. After passing through the Lombok Strait, the wave propagates northeastward through
 506 the Flores Sea, and then reaches the Pacific Ocean via the Banda Sea and the Molucca
 507 or Halmahera Seas.

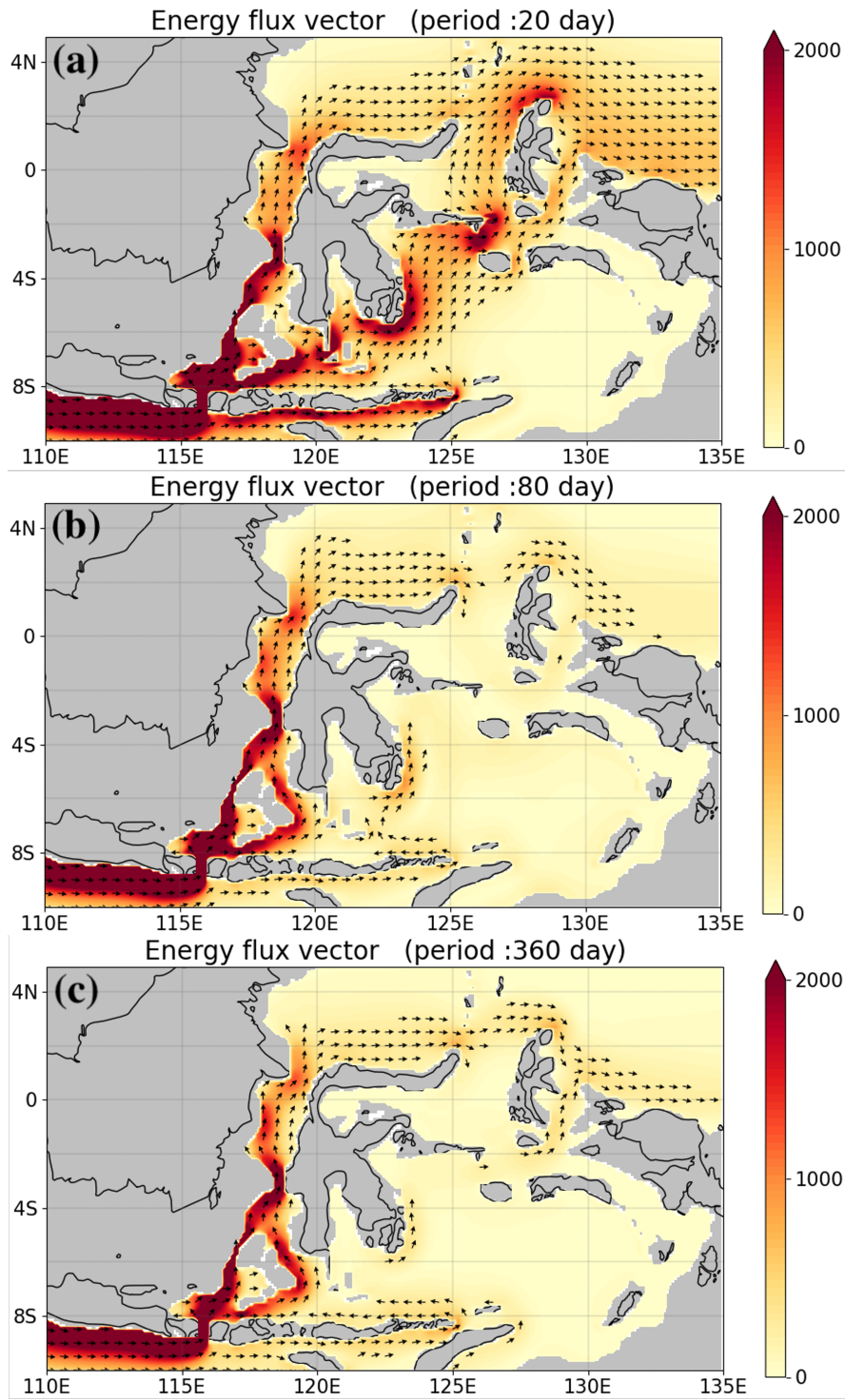


Figure 12. Horizontal distributions of the direction of energy flux vectors and magnitude of the energy flux within the Indonesian archipelago for the forcing period of (a) 20 days (b) 80 days, and (c) 360 days. Only the vectors with their magnitude larger than 200 W m^{-1} are shown.

508 The former pathway is found in all the experiments with various forcing periods. In con-
 509 trast, the latter is found only in the experiments with the period of zonal wind forcing
 510 shorter than 2 months.

511 Theoretical and observational studies have reported that the coastal Kelvin waves
 512 propagating along the southern coast of Java Island can reach the Ombai Strait and that
 513 the associated wave energy enters the Indonesian archipelago through the Ombai Strait,
 514 as well as the Lombok Strait (Sprintall et al., 2000; Durland & Qiu, 2003; Syamsudin
 515 et al., 2004). It is noted that, in the present study, about 65% of the incoming wave en-
 516 ergy passes through the Lombok Strait into the Indonesian archipelago except for the
 517 case with 10-day period forcing (not shown). This value is in good agreement with the
 518 results of Syamsudin et al. (2004), indicating $55.6 \pm 13.9\%$ from the altimeter data and
 519 65% from the model designed for the first baroclinic mode waves. In the case of 10day
 520 period forcing, only about 30% of the incoming energy passes through the Lombok Strait,
 521 which may be due to the strong energy dissipation caused by short wavelength.

522 4.3 Energy transmission rate

523 The differences in the properties of short-period and long-period waves also appear
 524 in the wave energy transmission rate. Fig. 13 shows the incoming wave energy from In-
 525 dian Ocean, E_{IO} , defined as the eastward energy flux across 110°E between 12°S and
 526 southern coast of Java Island (green line in Fig. 11a), the wave energy reaching the Pa-
 527 cific Ocean, E_{PA} , defined as the eastward energy flux across 140°E between 10°N and
 528 the northern coast of New Guinea Island (pink line in Fig. 11a), and transmission rate,
 529 E_{PA}/E_{IO} , for various period of the incoming waves. It is clearly shown that E_{IO} decreases
 530 as the forcing period increases, except for the shortest period of 10 days. This is con-
 531 sistent with the meridional energy partition of the equatorial Kelvin wave off the coast
 532 of Sumatra Island shown in Fig. 11c. The energy transmitted to the Pacific Ocean, E_{PA} ,
 533 also decreases as the period increases, but is almost constant for the periods longer than
 534 3 months. Thus, the transmission rate increases slightly with the forcing period for the
 535 periods longer than 3 months. In the experiments with the shorter period forcing, the
 536 transmission rate has a minimum value of about 12% at the 50-day period, while the max-
 537 imum of about 27% appears at the 20-day period. It can be said that this maximum trans-
 538 mission rate corresponds to the existence of the additional pathway for the shorter forc-
 539 ing period shown in Fig. 12a.

540 The energy transmission rate at high frequency in Fig. 13 does not agree with the
 541 result of one-dimensional wave interference problem through an ideal strait by Durland
 542 and Qiu (2003). They showed that the energy transmission rate increases monotonically
 543 as the wave period increases in a narrow channel-like passage similar to the Lombok Strait.
 544 In fact, the transmission rate only for the Lombok Strait in this study does not increase
 545 with the period either. However, because the obtained energy fluxes are time-averaged
 546 over one forcing period, the energy fluxes through the Lombok Strait are caused by su-
 547 perposition of the northward propagating energy directly from the Indian Ocean and the
 548 southward propagating energy returning to the Indian Ocean, which enters the Indone-
 549 sian archipelago through the Ombai Strait or the Timor Sea and propagates back as the
 550 coastal Kelvin waves. Therefore, our results do not represent a pure amount of the north-
 551 ward energy propagation through the Lombok Strait. In other words, the northward en-
 552 ergy propagation through the Lombok Strait in the realistic condition may be rather dif-
 553 ferent from the idealized case shown in Durland and Qiu (2003). In addition, the res-
 554 olution of our experiment, $1/10$ degrees, may be too coarse to consider the very narrow
 555 straits.

556 Since it is difficult to discuss the transmission rate by focusing on particular pas-
 557 sages, for example via the Lombok Strait as mentioned above, we consider the energy
 558 which goes across the equator to the north through the Makassar Strait ($E_{Makassar}$), the

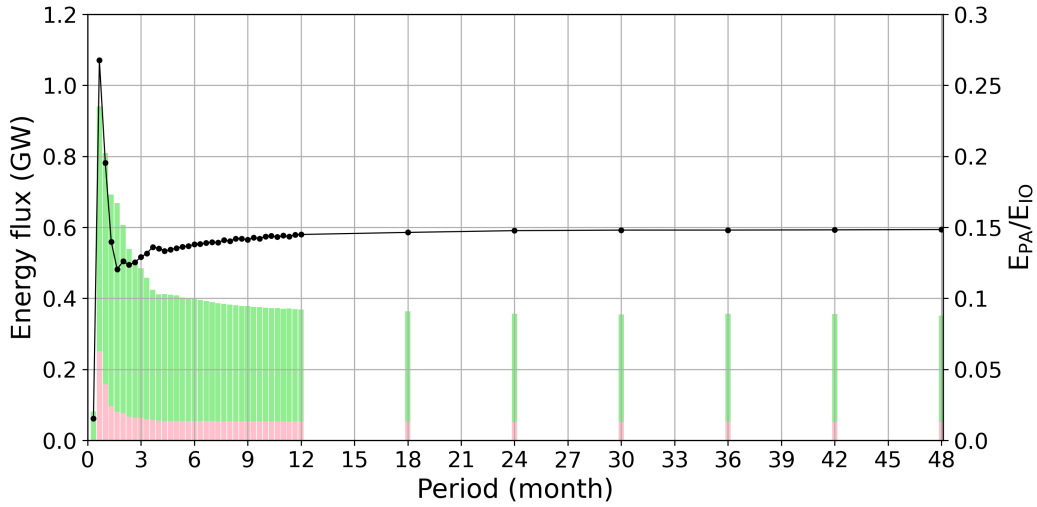


Figure 13. Incoming wave energy flux from the Indian Ocean E_{IO} (green), the wave energy reaching the Pacific Ocean E_{PA} (pink), and transmission rate E_{PA}/E_{IO} (solid line) as a function of the forcing period.

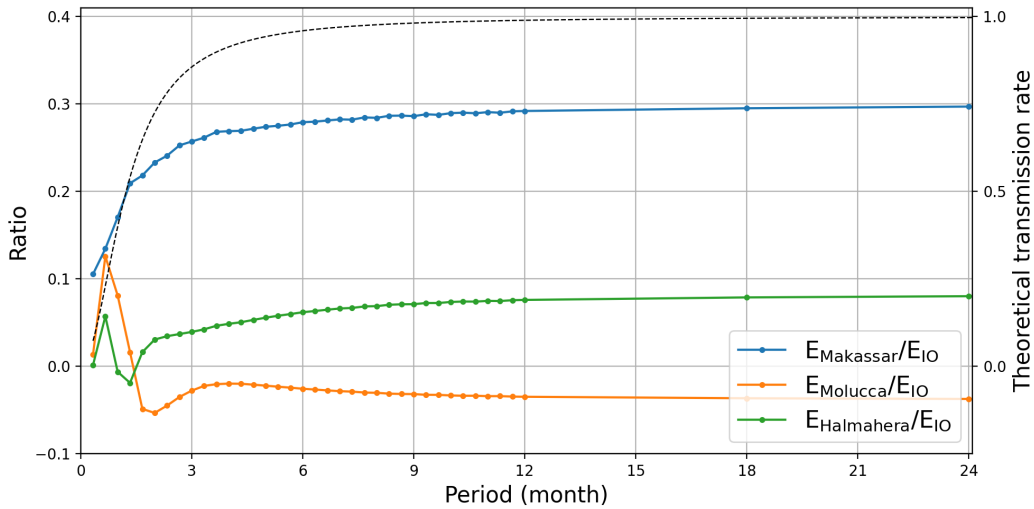


Figure 14. The ratio of the northward energy flux across the equator through the Makassar Strait ($E_{Makassar}$), the Molucca Sea ($E_{Molucca}$), and the Halmahera Sea ($E_{Halmahera}$) relative to the incoming wave energy from the Indian Ocean (E_{IO}) as a function of the forcing period (left axis). Theoretical wave energy transmission rates for each Kelvin wave period based on the Kelvin wave transmission theory (Durland & Qiu, 2003) (dashed line, right axis). The theoretical transmission rates are calculated for the narrowest part of the Makassar strait at 3°N , 50 km wide and 100 km long.

559 Molucca Sea (E_{Molucca}) and the Halmahera Sea ($E_{\text{Halmahera}}$). It is noted that the coastal
 560 Kelvin waves trapped around the islands, which are superimposed on the pure incom-
 561 ing waves, cannot cross the equator. Fig. 14 shows the transmission ratio of E_{Makassar} ,
 562 E_{Molucca} and $E_{\text{Halmahera}}$ to the incoming wave energy, propagating eastward off the south-
 563 ern coast of Java Island (E_{IO}). The transmission rate of the Makassar Strait increases
 564 as the wave period increases in the shorter periods and is almost constant in the longer
 565 periods. The Kelvin waves approaching to the Makassar Strait are not expected to pass
 566 smoothly, because the width of the strait at the narrowest part of the Makassar Strait
 567 is narrower than $1/5$ of the deformation radius. Fig. 14 also shows the theoretical en-
 568 ergy transmission rate through the Makassar Strait calculated based on the Kelvin wave
 569 transmission theory through the strait narrower than the deformation radius (Durland
 570 & Qiu, 2003). The energy transmission rate becomes smaller for shorter period Kelvin
 571 waves because the phase of the incoming Kelvin waves changes before the adjustment
 572 in the strait is completed. Comparing the theory (dashed line Fig. 14) and our results
 573 (blue line in Fig. 14), the energy transmission rate is almost constant for sufficiently long
 574 period in both cases. However, the constant values are very different: it's almost 1 in
 575 the theory while it's about 0.3 in the model results. This discrepancy may be due to the
 576 inability to accurately estimate the incoming energy into the Makassar Strait for the model
 577 result and to the lack of the viscous effect in the theory of Durland and Qiu (2003) as
 578 pointed out by Johnson and Garrett (2006). Nevertheless, their dependencies on the in-
 579 coming wave period show the similar tendency. Thus, it is reasonable to consider that
 580 the smaller energy transmission rate for the shorter period Kelvin waves in the model
 581 is due to incomplete adjustment in the strait with the faster phase change of the incom-
 582 ing Kelvin waves, as discussed in Durland and Qiu (2003).

583 Unlike the Makassar Strait, the transmission rates of the Molucca Sea and Halmahera
 584 Sea do not increase with increasing the period and have a maximum and a nega-
 585 tive minimum in the periods shorter than 3 months. This peculiar behavior may be re-
 586 lated to the complicated wave propagation around the Halmahera Island associated with
 587 the additional eastern pathway of the wave energy within the Indonesian archipelago.
 588 Fig. 14 also shows that the transmission rates of the Molucca Sea and Halmahera Sea
 589 are much smaller than that of the Makassar Strait in all the periods, suggesting the main
 590 route of the wave energy through the Makassar Strait. It is interesting to note that the
 591 sum of the transmission rate for the three passages in Fig. 14 is far less than 1, which
 592 seems to be caused by the effect of energy dissipation. Horizontal distributions of the
 593 energy dissipation rate indicates that the strong energy dissipation appears along the
 594 major route of the energy flux from the Lombok Strait to the Makassar Strait (not shown).
 595 The dissipation rate is larger in the west at each latitude within the archipelago, sug-
 596 gesting the importance of the western boundary layer as in the results of the Pacific ex-
 597 periments.

598 5 Summary and Discussion

599 The detailed pathways of the equatorial wave energy through the Indonesian archipelago
 600 and the processes responsible for the formation of the pathways are investigated using
 601 a 1.5-layer reduced gravity model, for the incoming waves both from the Pacific Ocean
 602 and from the Indian Ocean. The energy transmission rates between the two basins are
 603 also quantitatively explored for a wide range of the forcing period. In order to evaluate
 604 the wave energy flux in the equatorial region, the formulation proposed by Aiki et al.
 605 (2017) is utilized. This energy flux analysis scheme has enabled us to perform a unified
 606 treatment of the equatorial and mid-latitude Rossby waves and the equatorial and coastal
 607 Kelvin waves. It can also show directly how the energy of incoming waves from the Pa-
 608 cific Ocean reaches the Indian Ocean and vice versa.

609 For the case of incoming Rossby waves from the Pacific Ocean, most of the wave
 610 energy propagates southward through the Halmahera Sea and reaches the Indian Ocean

611 via the Banda and Timor Seas. It turns out that the wave energy propagating around
 612 the island chain in the Banda Sea cancels the southward energy flux along the eastern-
 613 most route and has the main pathway shifted to the western side of the island chain. An-
 614 other pathway to the Indian Ocean via the Makassar Strait also shows significant mag-
 615 nitude of energy flux, but the energy entering the Indonesian Seas through the Makas-
 616 sar Strait is about a quarter of the one through the Halmahera Sea. This wave energy
 617 flux distribution is different from the transport distribution of the ITF mean flow which
 618 enters the Indonesian archipelago mainly through the Makassar Strait (Gordon & Fine,
 619 1996; Gordon, 2005). Therefore, it is suggested that not only the western pathway via
 620 the Makassar Strait but also the eastern pathway via the Banda Sea should be consid-
 621 ered to investigate the impacts of the variabilities in the tropical Pacific Ocean on the
 622 Indonesian archipelago.

623 The energy budget analysis indicates that both the transmitted and reflected wave
 624 energy decreases significantly for the wave period shorter than 1.5 years, which is mainly
 625 due to the increase in energy dissipation along the northern coast of New Guinea. The
 626 different characteristics of the energy propagation for the shorter period waves may be
 627 related to the geometry of the western boundary of the equatorial Pacific Ocean. The
 628 zonal wavelength of the first meridional mode equatorial Rossby wave at the 1.5-year pe-
 629 riod is about 40,000 km, which is equivalent to about two times the zonal width of New
 630 Guinea. For this reason, the meridional wall approximation adopted by Clarke (1991)
 631 may be appropriate when the period of incoming Rossby wave is longer than 1.5-year.

632 The inclination of the New Guinea coast also affects mass flux along the coast. The
 633 reflection of the equatorial Rossby waves at the inclined western boundary has already
 634 investigated by considering mass flux normal to the coastline (Cane & Gent, 1984; Mc-
 635 Calpin, 1987). In these studies, the reflected short Rossby wave merely redistributes mass
 636 along the coastline, and the incoming mass flux of the incident Rossby wave and the out-
 637 going mass flux of the reflected Kelvin wave are balanced. When the western boundary
 638 is inclined, however, the total incoming mass flux normal to the coastline decreases be-
 639 cause the phase difference along the boundary induces incoming and outgoing mass fluxes
 640 simultaneously. This decrease of incoming mass flux becomes more important as the wave-
 641 length of the incident wave becomes shorter. Thus, the decrease of reflection rate with
 642 decreasing wave period shown in this study (see Fig. 7) is partly due to the change in
 643 the total mass flux balance along the western boundary. However, the reduction of re-
 644 flection rate in the present study is more rapid than that explained by the mass flux bal-
 645 ance only, and this difference may be explained by the energy dissipation in the bound-
 646 ary layer. The phase shift of the incoming mass flux along the western boundary causes
 647 the strong boundary flow to redistribute mass within the boundary layer. This bound-
 648 ary flow forms the strong horizontal velocity shear, which induces the large energy dis-
 649 sipation. Therefore, the reduction of reflection rate in the shorter period cases shown in
 650 Fig. 7 may be due to the change in the mass flux balance at the western boundary and
 651 to the energy dissipation associated with the enhanced boundary flow. Furthermore, our
 652 simple simulations show that incoming semiannual Rossby waves can excite intraseasonal
 653 Yanai wave at tilted western boundary (see Fig. 9b). This result suggests that the in-
 654 traseasonal Yanai waves near the western boundary are excited not only by direct wind
 655 forcing or instability as suggested by previous studies (e.g. Chatterjee et al., 2013), but
 656 also by reflection of the long Rossby waves with longer periods.

657 It is worth mentioning that additional experiments with advective terms show sim-
 658 ilar results with about 2% decrease in the transmission rate and about 2% increase in
 659 the reflection rate (not shown), therefore, nonlinear effects may have some influences on
 660 the Rossby wave reflection on the western boundary as suggested by Yuan and Han (2006);
 661 Yuan et al. (2019) and the wave intrusion into the Indonesian archipelago. Despite the
 662 decrease of wave energy entering the Indonesian archipelago, the behaviors of waves in
 663 the archipelago are similar to those in the linear experiments. It is also noted that the

664 nonlinear experiments in the present study do not include ITF like mean flow, thus no
665 wave-mean flow interaction is taken into account.

666 In the case of the Kelvin waves propagating from the equatorial Indian Ocean, about
667 half of the incident wave energy onto the eastern boundary for the period longer than
668 one month is distributed to the south off the western coast of Sumatra Island and con-
669 tinues propagating eastward along the Sumatra and Java Islands as the coastal Kelvin
670 waves. When the incoming wave period is shorter than one month, most of the wave en-
671 ergy is distributed to the south. The eastward coastal Kelvin waves enter the Indone-
672 sian Seas through the Lombok and Ombai Straits and propagate northward through the
673 Makassar Strait to reach the western Pacific. Another pathway to the western Pacific
674 via the Banda Sea appears clearly only when the incoming wave period is shorter than
675 2 months. The energy budget analysis indicates that about 15% of the incoming wave
676 energy reaches the western Pacific for the incoming wave period longer than 1 year. The
677 transmission rate also has a peak at 20-day period with a value of about 27%, correspond-
678 ing to the existence of the additional pathway. Considering such intraseasonal waves is
679 important because observed transport signal at ITF outflow passages suggest the Kelvin
680 waves forced by periodic winds with period of 28-46 days (Drushka et al., 2010).

681 The shorter period Kelvin waves from the Indian Ocean can enter the Indonesian
682 archipelago, much easier compared to the Rossby waves from the Pacific Ocean, and the
683 transparency of narrow straits play an important role on this difference. The straits nar-
684 rower than the deformation radius, such as the Lombok and Makassar Straits, tend to
685 suppress the transmission of the short-period waves (Durland & Qiu, 2003). Because this
686 suppression depends strongly on the ratio of deformation radius to the width of passage,
687 the location of the strait is important. The Makassar Strait is located at a lower lati-
688 tude than the Lombok Strait, thereby the deformation radius becomes larger at the Makas-
689 sar Strait. When the incoming Kelvin waves with a period of about one month enter the
690 Indonesian archipelago, much energy can propagate through the Lombok Strait, but not
691 through the Makassar Strait, where the strong energy dissipation occurs instead. This
692 may be the reason for the wave energy to reach the Pacific via the Banda Sea for the pe-
693 riod shorter than one month.

694 Most of the incident wave energy enters the Indonesian archipelago through the
695 Lombok Strait in the present study. The wave signals from the equatorial Indian Ocean,
696 however, have also been observed in the Ombai Strait (Molcard et al., 2001; Potemra et
697 al., 2002; Sprintall et al., 2009; Drushka et al., 2010). Drushka et al. (2010) suggest that
698 the Kelvin wave signals in the Ombai Strait is due to the downward propagation that
699 prevent the incoming Kelvin wave from passing through the shallow Lombok Strait. The
700 1.5-layer reduced gravity model does not include such vertical process, thus, may not be
701 sufficient for the realistic representations of the Kelvin wave penetration into the archipelago.
702 However, the high transmission rates and the additional eastern energy pathway for in-
703 traseasonal waves are still apparent in sensitivity experiments without the Lombok Strait
704 (not shown).

705 Although only 10% of the incoming wave energy from the Pacific Ocean reaches
706 the southeastern Indian Ocean, the wave signals from the Pacific Ocean certainly affect
707 the interannual variability in the Indian Ocean, such as the Leeuwin Current (Feng et
708 al., 2003) and the Ningaloo Niño (Kataoka et al., 2014). On the other hand, about 10%
709 of the incoming wave energy from the Indian Ocean reaches the Pacific Ocean in the present
710 study. However, the ocean waves from the Indian Ocean have not been observed in the
711 western Pacific Ocean. These differences of ocean waves in reality may be due to the dif-
712 ference in period of the dominant variations or intensities of the forcing between the Pa-
713 cific and Indian Oceans, which would be the important questions for future works.

Appendix A Formation of Energy Flux

Derivation of a new formulation of the energy flux proposed by Aiki et al. (2017) (hereafter AGC17) is briefly shown here. Following AGC17, we assume linear waves in the absence of a mean flow on an equatorial β -plane. Then, the linear shallow water equations are nondimensionalized, with the time scale of $1/\sqrt{c\beta}$ and length scale of $\sqrt{c/\beta}$, as:

$$\begin{aligned}\frac{\partial u}{\partial t} - yv + \frac{\partial p}{\partial x} &= 0 \\ \frac{\partial v}{\partial t} + yu + \frac{\partial p}{\partial y} &= 0 \\ \frac{\partial p}{\partial t} + \frac{\partial u}{\partial x} + \frac{\partial v}{\partial y} &= 0\end{aligned}\tag{A1}$$

where p indicates pressure. Manipulation of the equations A1 yields the wave energy equation

$$\frac{\partial}{\partial t}(u^2 + v^2 + p^2)/2 + \nabla \cdot \langle up, vp \rangle = 0\tag{A2}$$

where $\langle \cdot \rangle$ means a horizontal vector. According to this energy equation A2, the divergence of pressure flux, $\nabla \cdot \langle up, vp \rangle$, accurately represent the time rate of energy change at a particular location. However, the pressure flux itself does not always point in the direction of the group velocity vector, i.e.

$$\langle up, vp \rangle \neq \left\langle \frac{\partial \omega}{\partial k}, \frac{\partial \omega}{\partial l} \right\rangle (u^2 + v^2 + p^2)/2\tag{A3}$$

where ω is wave frequency, k and l are zonal and meridional wavenumber respectively. In mid-latitudes, this problem can be avoided by taking into account the pressure flux associated with geostrophic flows Orlanski and Sheldon (1993). In contrast, in equatorial regions, we cannot consider geostrophic flows. Therefore, another diagnostic quantity that represents the difference between the two sides of equation A3 is required to evaluate the energy flux.

(Matsuno, 1966) has derived a solution to equation A1 on the equatorial β -plane, which is shown as

$$\begin{aligned}v &= A \cos \theta \exp(-y^2/2) H^{(n)} \\ u &= (\omega y v_\theta - k v_{y\theta}) / (\omega^2 - k^2) \\ p &= (k y v_\theta - \omega v_{y\theta}) / (\omega^2 - k^2)\end{aligned}\tag{A4}$$

where A is wave amplitude, $H^{(n)}$ is the Helmite polynomial with n being the meridional mode number, θ is wave phase ($kx - \omega t$). The subscript represents partial differentiation. By using the solutions A4, phase averaged zonal pressure flux can be written as

$$\overline{up} = \overline{v\bar{v}}(2\omega k + 1)/[2(\omega^2 - k^2)] + [\overline{v_y\bar{v}}(2\omega k) - y\overline{v\bar{v}}(\omega^2 + k^2)]_y/[2(\omega^2 - k^2)^2]$$

where overbar denotes the phase average. In the same way, the wave energy can be decomposed into two parts,

$$\overline{(u^2 + v^2 + p^2)}/2 = \overline{v\bar{v}}(2\omega^2 + k/\omega)/[2(\omega^2 - k^2)] + [\overline{v_y\bar{v}}(\omega^2 + k^2) - y\overline{v\bar{v}}(2k\omega)]_y/[2(\omega^2 - k^2)^2]$$

Then we can obtain an analytical expression for difference between the right and left sides of A3 to yield

$$(\partial\omega/\partial k)\overline{(u^2 + v^2 + p^2)}/2 - \overline{up} = \frac{-(\overline{p\bar{v}\theta})_y - (2\overline{u_{tt}v\theta})_y}{2k(1 + 2\omega^3/k)}$$

Finally, the right hand side of the equation A3, i.e. zonal component of the group velocity times wave energy can be rewritten in phase averaged form:

$$(\partial\omega/\partial k)\overline{(u^2 + v^2 + p^2)}/2 = \overline{u\bar{p}} + (\overline{p\bar{\varphi}}/2 + \overline{u_{tt}\bar{\varphi}})_y$$

744

$$\varphi \equiv -v_\theta / (k + 2\omega^3) \quad (\text{A5})$$

745

746

Meridional component of the group velocity times wave energy can also be derived in the same way. Furthermore, the definition of φ , the equation A5, can be written as

$$\nabla^2 \varphi - y^2 \varphi - 3\varphi_{tt} = -v_\theta / \omega = q$$

747

748

749

750

751

where q is the Ertel's potential vorticity. Therefore the scalar quantity φ can be estimated without using Fourier analysis, and then we can diagnostically estimate energy flux vector even with coastal boundaries. Moreover the scalar quantity φ is also applicable to mid-latitude waves. Thus, we can trace wave propagations at all latitude with coastal boundary by using the AGC17 scheme.

752

753

754

755

756

757

In the present study, we use simplified energy flux, called as level-2 flux in AGC17, in order to reduce the computational cost. Note that the level-2 flux provides an approximate expression for energy flux based on the group velocity of both low- and high- frequency equatorial waves. To calculate the level-2 energy flux vector of AGC17 scheme, the following approximated inverse problem in dimensionalized form is solved numerically, using results obtained during the last forcing period of our simulations:

$$\nabla^2 \varphi^{app} - (f/c)^2 \varphi^{app} = q \quad (\text{A6})$$

758

759

760

where $q = \frac{\partial v}{\partial x} - \frac{\partial u}{\partial y} - (f/c^2)p$ is the linearized Ertel's potential vorticity and p indicates pressure. Then, using φ^{app} obtained by solving the equation A6, we calculate the level-2 energy flux vector in the dimensionalized form:

$$\overline{\mathbf{V}p} + \nabla \times (\overline{p\varphi^{app}}) / 2$$

761

where \mathbf{V} is horizontal velocity vector and overbar denotes the phase average.

762

Open Research Section

763

764

ETOPO1 1 Arc-Minute Global Relief Model data are provided by the National Oceanic and Atmospheric Administration at <https://www.ngdc.noaa.gov/mgg/global/>.

765

References

766

767

768

769

770

771

772

773

774

775

776

777

778

779

780

781

782

783

- Aiki, H., Greatbatch, R. J., & Claus, M. (2017). Towards a seamlessly diagnosable expression for the energy flux associated with both equatorial and mid-latitude waves. *Progress in Earth and Planetary Science*, 4(1), 1–18.
- Amante, C., & Eakins, B. W. (2009). Etopo1 arc-minute global relief model: procedures, data sources and analysis.
- Boulanger, J.-P., & Fu, L.-L. (1996). Evidence of boundary reflection of kelvin and first-mode rossby waves from topex/poseidon sea level data. *Journal of Geophysical Research: Oceans*, 101(C7), 16361–16371.
- Boulanger, J.-P., & Menkes, C. (1995). Propagation and reflection of long equatorial waves in the pacific ocean during the 1992–1993 el nino. *Journal of Geophysical Research: Oceans*, 100(C12), 25041–25059.
- Boulanger, J.-P., & Menkès, C. (1999). Long equatorial wave reflection in the pacific ocean from topex/poseidon data during the 1992–1998 period. *Climate dynamics*, 15(3), 205–225.
- Busalacchi, A. J., McPhaden, M. J., & Picaut, J. (1994). Variability in equatorial pacific sea surface topography during the verification phase of the topex/poseidon mission. *Journal of Geophysical Research: Oceans*, 99(C12), 24725–24738.

- 784 Cane, M. A., & Gent, P. R. (1984). Reflection of low-frequency equatorial waves at
785 arbitrary western boundaries. *Journal of Marine Research*, *42*(3), 487–502.
- 786 Chatterjee, A., Shankar, D., McCreary Jr, J., & Vinayachandran, P. (2013). Yanai
787 waves in the western equatorial indian ocean. *Journal of Geophysical Research:*
788 *Oceans*, *118*(3), 1556–1570.
- 789 Chen, G., Han, W., Li, Y., McPhaden, M. J., Chen, J., Wang, W., & Wang, D.
790 (2017). Strong intraseasonal variability of meridional currents near 5° n in
791 the eastern indian ocean: Characteristics and causes. *Journal of Physical*
792 *Oceanography*, *47*(5), 979–998.
- 793 Clarke, A. J. (1991). On the reflection and transmission of low-frequency energy at
794 the irregular western pacific ocean boundary. *Journal of Geophysical Research:*
795 *Oceans*, *96*(S01), 3289–3305.
- 796 Clarke, A. J., & Liu, X. (1994). Interannual sea level in the northern and eastern in-
797 dian ocean. *Journal of Physical Oceanography*, *24*(6), 1224–1235.
- 798 Drushka, K., Sprintall, J., Gille, S. T., & Brodjonegoro, I. (2010). Vertical structure
799 of kelvin waves in the indonesian throughflow exit passages. *Journal of Physi-*
800 *cal Oceanography*, *40*(9), 1965–1987.
- 801 Du Penhoat, Y., & Cane, M. A. (1991). Effect of low-latitude western boundary
802 gaps on the reflection of equatorial motions. *Journal of Geophysical Research:*
803 *Oceans*, *96*(S01), 3307–3322.
- 804 Durland, T. S., & Qiu, B. (2003). Transmission of subinertial kelvin waves through a
805 strait. *Journal of Physical Oceanography*, *33*(7), 1337–1350.
- 806 Feng, M., Meyers, G., Pearce, A., & Wijffels, S. (2003). Annual and interannual
807 variations of the leeuwin current at 32 s. *Journal of Geophysical Research:*
808 *Oceans*, *108*(C11).
- 809 Gordon, A. L. (1986). Interocean exchange of thermocline water. *Journal of Geo-*
810 *physical Research: Oceans*, *91*(C4), 5037–5046.
- 811 Gordon, A. L. (2005). Oceanography of the indonesian seas and their throughflow.
812 *Oceanography*, *18*(4), 14–27.
- 813 Gordon, A. L., & Fine, R. A. (1996). Pathways of water between the pacific and in-
814 dian oceans in the indonesian seas. *Nature*, *379*(6561), 146–149.
- 815 Gordon, A. L., Susanto, R. D., & Field, A. (1999). Throughflow within makassar
816 strait. *Geophysical Research Letters*, *26*(21), 3325–3328.
- 817 Hendon, H. H., Liebmann, B., & Glick, J. D. (1998). Oceanic kelvin waves and
818 the madden–julian oscillation. *Journal of the Atmospheric Sciences*, *55*(1), 88–
819 101.
- 820 Johnson, H. L., & Garrett, C. (2006). What fraction of a kelvin wave incident on
821 a narrow strait is transmitted? *Journal of Physical Oceanography*, *36*(5), 945–
822 954.
- 823 Kataoka, T., Tozuka, T., Behera, S., & Yamagata, T. (2014). On the ningaloo
824 niño/niña. *Climate dynamics*, *43*(5-6), 1463–1482.
- 825 Li, J., & Clarke, A. J. (2004). Coastline direction, interannual flow, and the strong
826 el niño currents along australia’s nearly zonal southern coast. *Journal of Physi-*
827 *cal Oceanography*, *34*(11), 2373–2381.
- 828 Li, X., Yuan, D., Wang, Z., Li, Y., Corvianawatie, C., Surinati, D., . . . others
829 (2020). Moored observations of transport and variability of halmahera sea
830 currents. *Journal of Physical Oceanography*, *50*(2), 471–488.
- 831 Li, Z., & Aiki, H. (2020). The life cycle of annual waves in the indian ocean as iden-
832 tified by seamless diagnosis of the energy flux. *Geophysical Research Letters*,
833 *47*(2), e2019GL085670.
- 834 Madden, R. A., & Julian, P. R. (1994). Observations of the 40–50-day tropical oscil-
835 lation—a review. *Monthly weather review*, *122*(5), 814–837.
- 836 Matsuno, T. (1966). Quasi-geostrophic motions in the equatorial area. *Journal of*
837 *the Meteorological Society of Japan. Ser. II*, *44*(1), 25–43.
- 838 McCalpin, J. D. (1987). A note on the reflection of low-frequency equatorial rossby

- 839 waves from realistic western boundaries. *Journal of Physical Oceanography*,
840 17(11), 1944–1949.
- 841 Molcard, R., Fieux, M., & Syamsudin, F. (2001). The throughflow within ombai
842 strait. *Deep Sea Research Part I: Oceanographic Research Papers*, 48(5), 1237–
843 1253.
- 844 Murtugudde, R., Busalacchi, A. J., & Beauchamp, J. (1998). Seasonal-to-interannual
845 effects of the indonesian throughflow on the tropical indo-pacific basin. *Journal*
846 *of Geophysical Research: Oceans*, 103(C10), 21425–21441.
- 847 Orlandi, I., & Sheldon, J. (1993). A case of downstream baroclinic development
848 over western north america. *Monthly Weather Review*, 121(11), 2929–2950.
- 849 Potemra, J. T. (2001). Contribution of equatorial pacific winds to southern tropical
850 indian ocean rossby waves. *Journal of Geophysical Research: Oceans*, 106(C2),
851 2407–2422.
- 852 Potemra, J. T., Hautala, S. L., Sprintall, J., & Pandoe, W. (2002). Interaction be-
853 tween the indonesian seas and the indian ocean in observations and numerical
854 models. *Journal of Physical Oceanography*, 32(6), 1838–1854.
- 855 Pujiana, K., Gordon, A. L., & Sprintall, J. (2013). Intraseasonal kelvin wave in
856 makassar strait. *Journal of Geophysical Research: Oceans*, 118(4), 2023–2034.
- 857 Qiu, B., Mao, M., & Kashino, Y. (1999). Intraseasonal variability in the indo-pacific
858 throughflow and the regions surrounding the indonesian seas. *Journal of Physi-*
859 *cal Oceanography*, 29(7), 1599–1618.
- 860 Qu, T., Gan, J., Ishida, A., Kashino, Y., & Tozuka, T. (2008). Semiannual variation
861 in the western tropical pacific ocean. *Geophysical Research Letters*, 35(16).
- 862 Schiller, A., Wijffels, S., Sprintall, J., Molcard, R., & Oke, P. R. (2010). Pathways of
863 intraseasonal variability in the indonesian throughflow region. *Dynamics of at-*
864 *mospheres and oceans*, 50(2), 174–200.
- 865 Sloyan, B. M., & Rintoul, S. R. (2001). Circulation, renewal, and modification
866 of antarctic mode and intermediate water. *Journal of Physical Oceanography*,
867 31(4), 1005–1030.
- 868 Spall, M. A., & Pedlosky, J. (2005). Reflection and transmission of equatorial rossby
869 waves. *Journal of Physical Oceanography*, 35(3), 363–373.
- 870 Sprintall, J., Gordon, A. L., Murtugudde, R., & Susanto, R. D. (2000). A semian-
871 nual indian ocean forced kelvin wave observed in the indonesian seas in may
872 1997. *Journal of Geophysical Research: Oceans*, 105(C7), 17217–17230.
- 873 Sprintall, J., Wijffels, S. E., Molcard, R., & Jaya, I. (2009). Direct estimates of the
874 indonesian throughflow entering the indian ocean: 2004–2006. *Journal of Geo-*
875 *physical Research: Oceans*, 114(C7).
- 876 Suarez, M. J., & Schopf, P. S. (1988). A delayed action oscillator for enso. *Journal*
877 *of Atmospheric Sciences*, 45(21), 3283–3287.
- 878 Syamsudin, F., Kaneko, A., & Haidvogel, D. B. (2004). Numerical and observational
879 estimates of indian ocean kelvin wave intrusion into lombok strait. *Geophysical*
880 *research letters*, 31(24).
- 881 Wijffels, S., & Meyers, G. (2004). An intersection of oceanic waveguides: Vari-
882 ability in the indonesian throughflow region. *Journal of Physical Oceanogra-*
883 *phy*, 34(5), 1232–1253.
- 884 Wyrski, K. (1987). Indonesian through flow and the associated pressure gradient.
885 *Journal of Geophysical Research: Oceans*, 92(C12), 12941–12946.
- 886 Yuan, D., & Han, W. (2006). Roles of equatorial waves and western boundary reflec-
887 tion in the seasonal circulation of the equatorial indian ocean. *Journal of Physi-*
888 *cal Oceanography*, 36(5), 930–944.
- 889 Yuan, D., Hu, X., Xu, P., Zhao, X., Masumoto, Y., & Han, W. (2018). The iod-enso
890 precursory teleconnection over the tropical indo-pacific ocean: dynamics and
891 long-term trends under global warming. *Journal of Oceanology and Limnology*,
892 36(1), 4–19.
- 893 Yuan, D., Song, X., Yang, Y., & Dewar, W. K. (2019). Dynamics of mesoscale ed-

894 dies interacting with a western boundary current flowing by a gap. *Journal of*
895 *Geophysical Research: Oceans*, 124(6), 4117–4132.
896 Zhang, C., Hendon, H. H., Kessler, W. S., & Rosati, A. J. (2001). A workshop on
897 the mjo and enso. *Bulletin of the American Meteorological Society*, 82(5), 971–
898 976.